THE FLORIDA STATE UNIVERSITY

COLLEGE OF ARTS AND SCIENCES

CYCLONE SURFACE PRESSURE FIELDS AND FRONTOGENESIS FROM NASA SCATTEROMETER (NSCAT) WINDS

by

DAVID F. ZIERDEN

A Thesis submitted to the
Department of Meteorology
in partial fulfillment of the
requirements for the degree of
Master of Science

Degree Awarded:
Fall Semester, 1998

Degree Awarded:
Fall Semester, 1998

The members of the Committee approve the thesis of David F. Zierden defended on November 10, 1998.

James J. O'Brien
Professor Directing Thesis

John E. Ahlquist
Committee Member

Eric A. Smith
Committee Member

Mark A. Bourassa
Outside Committee Member

ACKNOWLEDGEMENTS

I would like to thank Dr. James J. O'Brien and particularly Dr. Mark A. Bourassa for their help and guidance in this research. Funding for this project is from the NASA JPL NSCAT project. COAPS recieves its base funding from ONR's Secretary of the Navy Grant to Dr. James J. O'Brien.

TABLE OF CONTENTS

LIST OF TABLES

LIST OF FIGURES

19.	NSCAT Vorticity 1800 UTC 5 January 1997	46
20.	GOES-9 Visible 1800 UTC 5 January 1997	47

ABSTRACT

Two extratropical marine cyclones and their associated frontal features are examined by computing surface pressure fields from NASA scatterometer (NSCAT) winds. A variational method blends high resolution (25 km) vorticity computed along the satellite track with an initial geostrophic vorticity field, resulting in a new geostrophic stream function and surface pressure field. Employing this method with each successive pass of the satellite over the study area allows this surface pressure field to evolve as dictated by the vorticity computed from NSCAT winds. The result is a high resolution surface pressure field that captures features such as fronts and low pressure centers in more detail than NCEP analyses. In addition, the high resolution vorticity fields computed from NSCAT winds reveal the location of surface fronts in great detail. These fronts are verified using NCEP analyses, *in situ* data, and satellite imagery.

CHAPTER 1

INTRODUCTION

The lack of conventional data over the oceans has long been a limiting factor in the accuracy of weather forecasting. Often, the only data available were surface observations from ships and buoys, which are sparse outside shipping lanes and the TOGA-TAO buoy array. Conventional data are now supplemented with satellite data and the challenge lies in finding new methods to best utilize these new data sources. One such source is surface wind measurements from spaceborn scatterometers. Scatterometer winds are currently assimilated directly into numerical weather prediction models with some success [*Hoffman*, 1993; *Andrews and Bell*, 1998]. The assimilation techniques insert winds at the surface and empirical methods are then needed to adjust higher atmospheric levels in the model. Surface pressures, on the other hand, can be assimilated directly and influence all levels of the atmosphere [*Atlas*, 1998].

The NASA Scatterometer (NSCAT) was operational from late September 1996 through June 1997. NSCAT yielded surface wind observations with greater accuracy, improved resolution, and better coverage than previous scatterometers. These data provide a powerful tool to aid in the identification of cyclones and fronts over remote areas of the ocean.

This study makes use of the high quality NSCAT wind data by deducing surface pressure fields through the use of a variational method. The primary goals are:

1) Use NSCAT winds to determine surface pressure fields,

pressure fields through the use of a variational method. The primary goals are:

1) Use NSCAT winds to determine surface pressure fields,

2) Follow the evolution of surface features described mostly with NSCAT data,

3) Identify and locate surface fronts,

4) Demonstrate a simple method for determining surface pressure fields from NSCAT winds, which can then be used for assimilation into NWP models.

An overview of scatterometry, including the specifics of NSCAT and the uses for scatterometer data, is presented in Chapter 2. Chapter 3 describes the data sets and details the variational method used to determine surface pressures. NSCAT surface pressure fields are then used to follow a case of cyclogenesis and a case of frontogenesis in the North Pacific (Chapter 4). Results show that the NSCAT pressure fields resolve the structure of these features in more detail than NCEP reanalyses. The NSCAT fields also agree better with NSCAT winds as far as the location of cyclone centers and the orientation of horizontal pressure gradients are concerned. Quantitatively, the NSCAT pressure fields compare well with NCEP, especially near the reference buoys and where recent satellite data are available. The signature of fronts in NSCAT relative vorticity is explored (Chapter 5). Linear bands of high relative vorticity values are verified as fronts using surface temperature gradients from independent measurements and visible satellite imagery.

CHAPTER 2

BACKGROUND

2.1 Scatterometry

Spaceborn scatterometers are active microwave sensors used to derive the speed and direction of surface winds. Active microwave radars transmit pulses to the earth's surface, then measure the strength of the back-scattered signal. Over the ocean's surface, the signal is Bragg scattered by ultragravity waves (waves with both surface tension and gravity as restoring forces). Although the relationship between wind speed and surface roughness is highly complex and not fully understood at this time, the radar returns and surface winds are highly correlated making accurate retrieval possible. Furthermore, the backscatter is anisotropic, which makes retrieval of wind direction possible through the use of multiple viewing angles.

Historically, the correct determination of wind direction has presented the greatest problem in scatterometry. As a low, polar-orbiting satellite passes over an area, a point can be viewed from multiple angles within five minutes, usually between 45 and 135 degrees. A mathematical function relating the strength of the backscatter, measured from the different angles, to wind direction has multiple minima, called ambiguities [*Freilich and Dunbar*, 1992; *Offiler*, 1994]. In the absence of noise, the best fit should correspond to the true wind direction, the next best fit to roughly 180 degrees opposite, and the others (if any) to around 90 degrees perpendicular to the true wind direction. However, noise in measured return signals can at times cause selection of the wrong ambiguity, (also called an

any) to around 90 degrees perpendicular to the true wind direction. However, noise in measured return signals can at times cause selection of the wrong ambiguity, (also called an

alias). Algorithms have been developed to identify and correct some of these aliases by checking for space and time continuity and by comparison to independent fields such as model output [*Stoffelen and Anderson,* 1997; *Offiler*, 1994; *Gonzales and Long*, 1988].

It has also been shown that for some scatterometers, wind speed measurements are biased at low and high wind speeds. *Jones et al.* [1982] assert that low wind speeds are underestimated and high wind speeds are overestimated by the Seasat-A Scatterometer, in a comparison using accurate ground truth measurements made during the JASIN study. The opposite is true for many model functions used for the ERS-1 scatterometer [*Rufenach,* 1998; *Boutin and Etechto,* 1996]. The NASA scatterometer (NSCAT), however, shows no evidence of this problem in its wind data.

2.2 NASA Scatterometer (NSCAT)

The data used in this study are from the NASA Scatterometer (NSCAT), which operated aboard Japan's ADEOS satellite for nine months from late September 1996 through June 1997. NSCAT was the first of a new generation of scatterometers, and it used many technological advances to improve the quality, coverage, and resolution of near surface winds. NSCAT's radar operated in the Ku-band (13.995 GHz) rather than the C-band as ERS-1 and Seasat-A. This frequency led to greater accuracy at low wind speeds (< 4 m/s), although sensitivity to attenuation by liquid water was increased. Engineering advancements in the sensors increased the signal to noise ratio of the backscatter measurements, greatly improving ambiguity selection. In addition, each wind cell was viewed from three different angles (figure 1). Seasat-A only employed two antenna sets. The third angle provided an independent measurement that aided in ambiguity selection. In addition, NSCAT was equipped to measure backscatter on both sides of the satellite track, doubling the coverage of ERS-1 that viewed only one side. The NSCAT radar was

In addition, NSCAT was equipped to measure backscatter on both sides of the satellite track, doubling the coverage of ERS-1 that viewed only one side. The NSCAT radar was

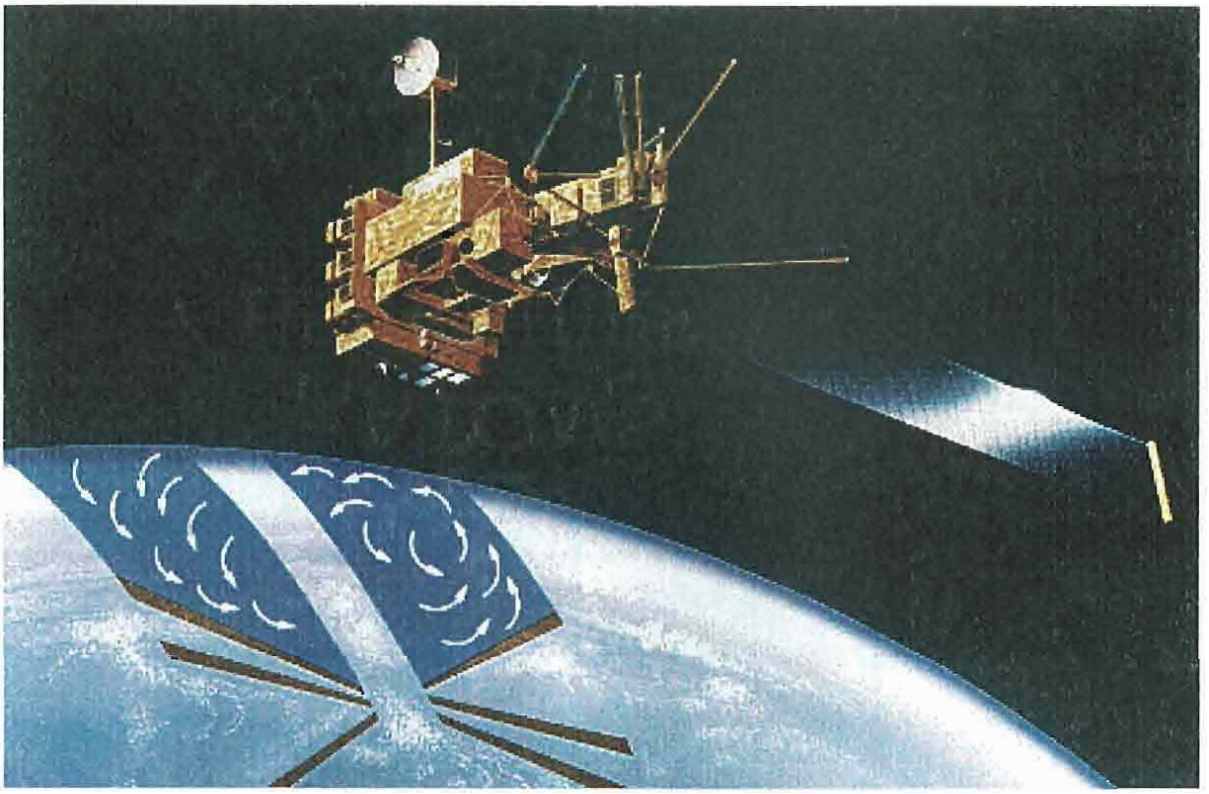

Figure 1. Schematic of the ADEOS satellite and antennae used for the NSCAT scatterometer. Figure is used courtesy of the Jet Propulsion Laboratory.

dual-polarized, and provided additional measurements (from one antenna) to improve ambiguity selection.

A digital Doppler filter grouped overlapping backscatter measurements from the different viewing angles into 25 km by 25 km cells. Seasat-A, on the other hand, used a crystal analog filter that contributed to data gaps by failing to properly overlap measurements from the fore and aft antennae. The wind speed and direction were computed for each cell using the observed backscatters and a lookup table. High quality *in situ* surface observations from new NDBC buoys, the TOGA-TAO array, and research vessels made calibration/validation of the model function more accurate than previous scatterometers. In particular, *in situ* surface wind data from the tropical Pacific included

vessels made calibration/validation of the model function more accurate than previous scatterometers. In particular, *in situ* surface wind data from the tropical Pacific included

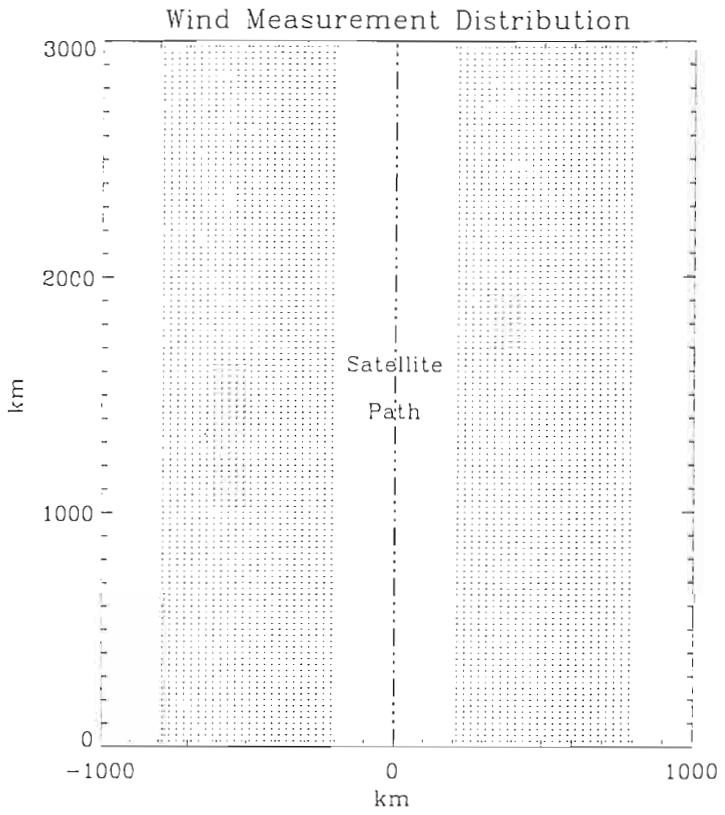

Figure 2. Data coverage and resolution along the path of the ADEOS satellite. Dots mark the relative location of each wind sample.

many observations at low wind speeds, enabling accurate calibration/valitation and removing the low wind speed biases that are found in other scatterometers.

Attenuation by liquid water in the atmosphere, particularly heavy precipitation, is a disadvantage of the Ku-band frequency. Contamination from precipitation droplets can significantly degrade the quality of scatterometer-computed wind vectors. Ideally, inclusion of a passive microwave radiometer on the satellite platform could identify contaminated cells and flag them appropriately. Unfortunately, mission specifications and funding did not allow for such an instrument to be included with NSCAT, so there is no

contaminated cells and flag them appropriately. Unfortunately, mission specifications and funding did not allow for such an instrument to be included with NSCAT, so there is no

way to identify contimated cells. Studies are ongoing to determine the effects of precipitation on the overall accuracy of the NSCAT winds.

The ADEOS satellite was a low altitude, sun-synchronous, near polar orbiter. In this orbit NSCAT covered 90 percent of the ice-free ocean in two days. The antenna configuration allowed winds to be measured in 600 km wide swaths on each side of the satellite, with a 400 km gap in the nadir view between the swaths (Figure 2). NSCAT level II (W25) wind data covered swaths on each side of the satellite, each swath 24 cells wide. These rows of 24 cells were perpendicular to the satellite's path (Figure 2).

NSCAT proved to be a very reliable instrument, determining near-surface winds (calibrated to a height of 10 m) more accurately and with fewer aliases than previous scatterometers. The chances of selecting an incorrect ambiguity were negligible at wind speeds over 8 m/s [*Bourassa et al.*, 1997]. Below that threshold the chances of incorrect ambiguity selection increased with decreasing wind speed. *Bourassa et al.* [1997] compared NSCAT winds to high frequency observations made by research vessels over a wide range of latitudes. The root mean square (RMS) difference between NSCAT and research vessel winds was found to be 1.6 m/s for wind speed ($U_{10} > 4$ m/s) and 13 degrees for direction. They found no statistically significant biases at low or high wind speeds.

2.3 Uses for Scatterometer Data

NSCAT and other scatterometers provided wind measurements over the ocean with much greater resolution and coverage than were previously available. Recent research looked to find ways to utilize this high quality data source. A common approach was to form gridded products [*Bourassa et al.*, 1998; *Liu et al.*, 1998]. The gridding looked to find ways to utilize this high quality data source. A common approach was to form gridded products [*Bourassa et al.*, 1998; *Liu et al.*, 1998]. The gridding

methodology of *Bourassa et al.* involved binning measurements from multiple passes of the satellite into cells, then performing a weighted temporal average. This method created daily fields on a 1 degree grid. A variety of methods were used to create weekly or monthly gridded products [*Liu et al.,* 1998; *Verschell et al.*, 1998]. These gridded products were used to drive ocean circulation models, improve surface fluxes for general circulation models, and to study the daily evolution of regional winds. Numerical weather prediction (NWP) models also assimilated scatterometer winds directly [*Thepaut et al.*, 1993]. Assimilation of ERS-1 winds into the ECMWF model impacted their forecasts only marginally [*Hoffman*, 1993]. *Andrews and Bell* [1998] demonstrated marked improvements in the UKMO forecasts by assimilating ERS-1 winds, particularly over the Southern Ocean where conventional data are sparse. While the above approaches utilized the global coverage and good temporal resolution of scatterometer winds, they did not take full advantage of the excellent spatial resolution of scatterometer wind data (25 km for NSCAT).

Some studies have employed scatterometer winds in diagnostic studies of mid-latitude and tropical cyclones. In many of these studies scatterometer data was only one of many data sources implemented in improving NWP analyses of the feature [*Anthes et al.*,1983; *Tomassini et al.,* 1998; *Liu et al.,* 1998]. In contrast, *Harlan and O'Brien* [1986] assimilated only Seasat-A scatterometer data with NMC pressure fields to obtain an improved estimate of central pressure in the QE-II storm of 1978. All these studies concentrated on improving estimates of the central surface pressure of the systems, but were not as concerned with the structure and evolution of the systems.

Brown and Zeng [1994] have done some promising work in computing surface pressure fields in mid-latitude cyclones using ERS-1 winds from a single swath and a boundary layer model. Surface gradient winds were found using ERS-1 wind data as input
pressure fields in mid-latitude cyclones using ERS-1 winds from a single swath and a boundary layer model. Surface gradient winds were found using ERS-1 wind data as input

to the boundary layer model. Surface pressures were then computed from the gradient winds and a reference pressure located within the field. The computed surface pressure fields distinguished fronts and located the centers of cyclones accurately while giving improved estimates of central pressure over the NMC analyses. The strength of their approach was twofold: (1) the surface pressure field was derived almost exclusively from scatterometer data and (2) swath data was used directly, without averaging in space or time. The drawback was that pressures can only be computed within the swath of wind data.

CHAPTER 3

DATA AND METHODOLOGY

A goal of this study is to devise a technique of deriving surface pressure fields from NSCAT winds, which have greater coverage and better resolution than ERS-1 winds. Like *Brown and Zeng* [1994], individual swath data are used, preserving the spatial resolution and small scale features present in NSCAT winds. Unlike *Brown and Zeng* [1994], any data within the domain has an influence on the entire field. Also, the surface pressure field will evolve in time with each additional satellite additional pass over the domain.

The primary data used in this study are NSCAT level II W25 winds. These winds have a resolution of 25 km and form a nearly continuous stream of data along the satellite's path from October 1996 through June 1997. National Center for Environmental Prediction (NCEP) reanalysis mean sea level pressures are also used to initialize the pressure field and to update boundary conditions. The NCEP mean sea level pressure data are available on a 2.5 degree global grid at 6 hour intervals. A third data source is *in situ* surface pressures from National Data Buoy Center (NCDC) buoys number 46003, located at latitude 51° 51' 5" N and longitude 20 5' 3" E, and 51001, located at latitude 23° 24' 4" N and longitude 197° 34' 1" E.

A study area is the North Pacific Ocean between 20°N and 55°N latitude and 165°E and 225°E longitude. This area is chosen for a number of reasons. It is largely free of land and ice (scatterometers work only over water) and large enough to capture synoptic-scale

ice (scatterometers work only over water) and large enough to capture synoptic-scale

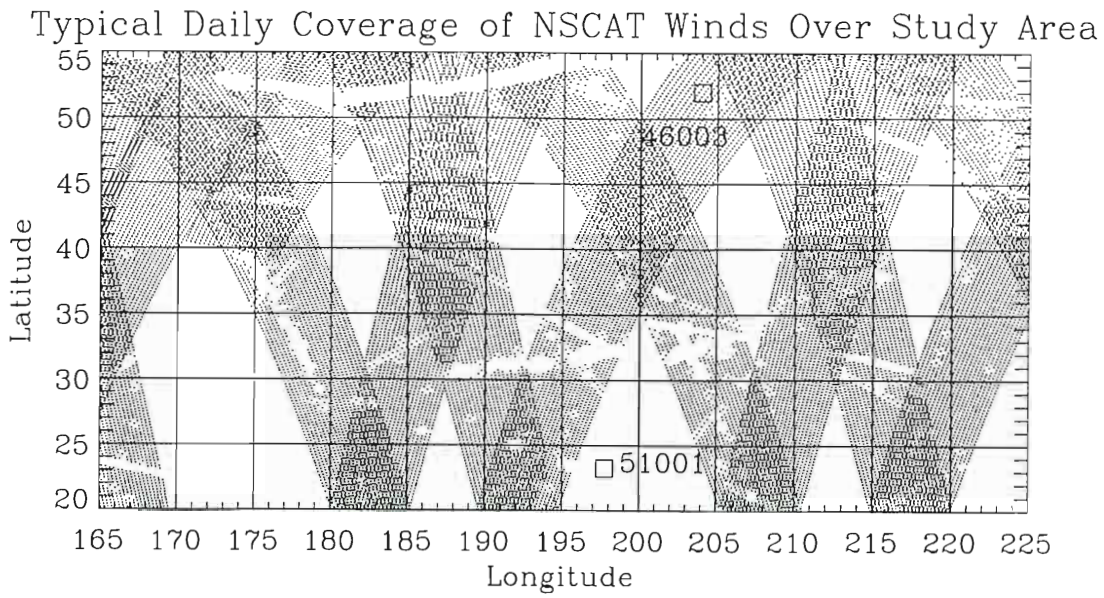

Figure 3. Typical daily coverage of NSCAT winds over the study area. Gaps within the swaths indicate missing data. NCDC buoy locations are marked with a square.

systems. Mid-latitude cyclones track through the region. Furthermore, conventional data are sparse and numerical weather prediction analyses can use improvement in this area. The study area could expect to see 3 to 4 passes of the satellite in the ascending node and another 3 to 4 passes in the descending node each day (Figure 3). All computations and analyses are performed on a 0.25° grid over the domain, preserving the small-scale features present in the high resolution NSCAT winds.

The technique developed in this study builds on the strengths of *Brown and Zeng* [1994] and incorporates the variational method of *Harlan and O'Brien* [1986]. The procedure (figure 4) begins with an NCEP mean sea level pressure field and interpolates it onto the 0.25° grid over the domain. For each subsequent pass of the satellite over the study area, the two swaths of NSCAT wind data are assimilated into the pressure field. Although surface pressure and winds are physically different data types, they are related

study area, the two swaths of NSCAT wind data are assimilated into the pressure field. Although surface pressure and winds are physically different data types, they are related

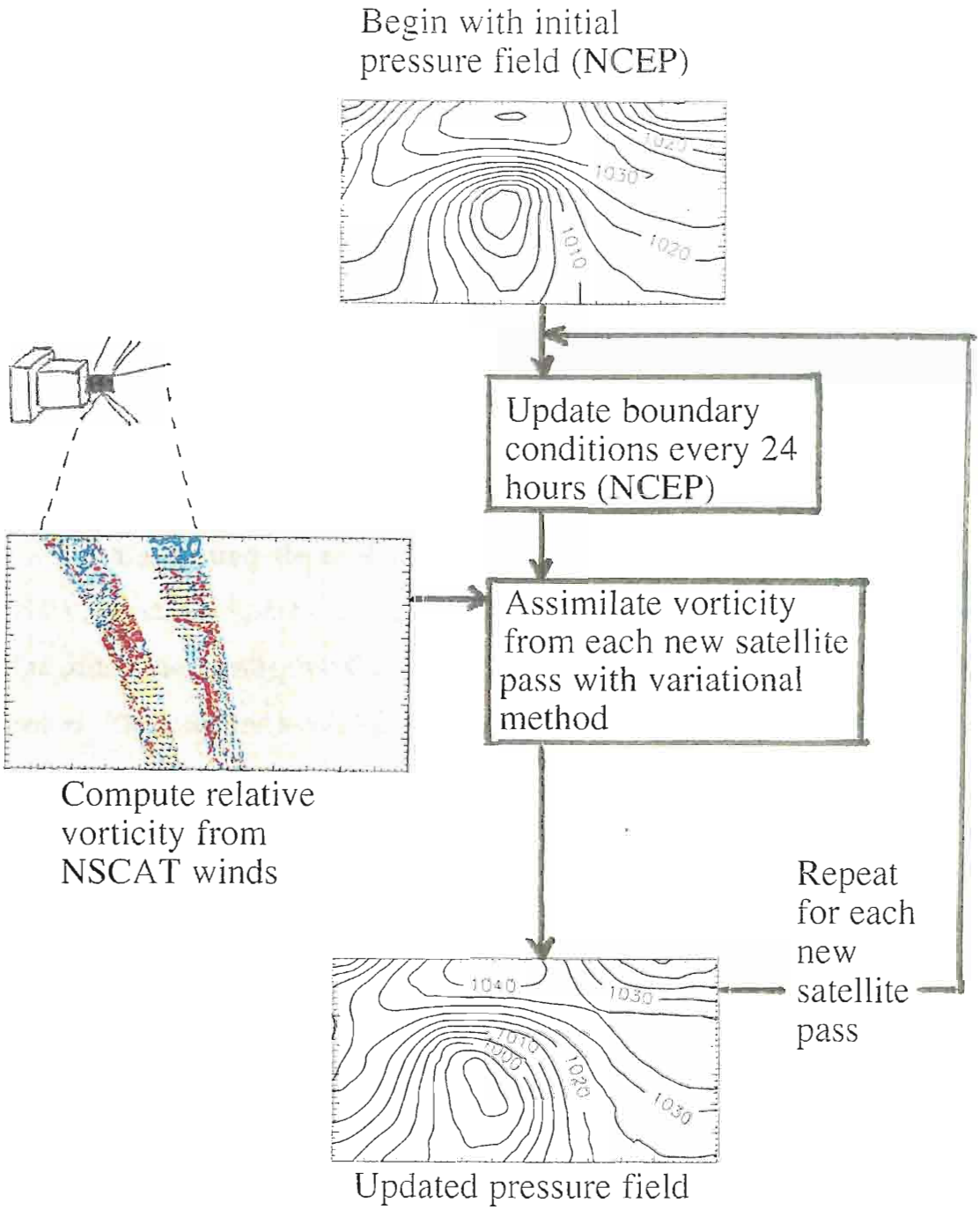

Figure 4. Methodology of computing surface pressure fields from NSCAT winds.

through vorticity. Relative vorticity is computed in the swaths from NSCAT winds, and then interpolated to the 0.25° domain grid, while geostrophic vorticity is computed from the pressure field. A variational method solves for a new geostrophic stream function, minimizing the difference between the new geostrophic vorticity and NSCAT vorticity where satellite data are present, and minimizing the difference between the new geostrophic vorticity and old geostrophic vorticity where no satellite data are present. The result is an updated pressure field that captures the features found in the NSCAT vorticity. Repeating this procedure with each new pass of the satellite over the domain allows the field to evolve in time as dictated by NSCAT data. All the steps of this procedure are described in detail in the following sections.

3.1 Computing Relative (NSCAT) and Geostrophic Vorticity

NSCAT winds are of high spatial density and located on a regular grid along the satellite path; consequently, relative vorticity is easily computed using centered finite differences. The speed and azimuthal direction of the winds are converted to across track (u') and along track (v') velocity components in a coordinate system aligned with the satellite track. The relative vorticity (ζ_S) at each interior point of the two swaths is

$$\zeta_{S\,ij} = (v'_{i+1,j} - v'_{i-1,j})/\Delta x' - (u'_{i,j+1} - u'_{i,j-1})/\Delta y' , \qquad (1)$$

where i denotes cell position across the swath, j denotes cell position along the swath, and x' and y' are across track and along track locations. $\Delta x'$ and $\Delta y'$ are twice the grid size and are computed directly from the latitude and longitude of the corresponding data points instead of being held constant at 50 km. They varied between 49 and 51 km. If wind data are missing at any of the necessary cells, the vorticity at that point is considered missing. Delunay triangulation and interpolation [*Renka*, 1982] then transfers the satellite vorticity

are missing at any of the necessary cells, the vorticity at that point is considered missing. Delunay triangulation and interpolation [*Renka*, 1982] then transfers the satellite vorticity

on to the 0.25° grid.

The RMS difference in NSCAT wind speeds is approximately of 1.5 m/s when compared to *in situ* data [*Bourassa et al.*, 1997; *Frielich and Dunbar,* 1998]. This uncertainty propagates through vorticity calculations and results in an uncertainty in relative vorticity of roughly 1 x 10^{-4} s^{-1}, similar in magnitude to large vorticity values. However, this RMS uncertainty in NSCAT wind speeds includes systematic biases and random errors in both NSCAT winds and the *in situ* data. Since relative vorticity involves the difference in u and v components, most of the uncertainty in vorticity is due to random error in NSCAT winds. The consistency of NSCAT vorticity fields with surface features and NCEP geostrophic vorticity suggests that random errors are small (< 0.7 m/s) and that the uncertainty in relative vorticity values is also small (< 1 x 10^{-5}).

Geostrophic vorticity is determined from surface pressure via a geostrophic stream function (Q):

$$Q_{ij} = \frac{p_{ij}}{\rho f}, \tag{2}$$

where p_{ij} is the surface pressure at each point, ρ is taken as a constant 1.225 kg/m^3 (U. S. Standard atmosphere), and f is the Coriolis parameter. Geostrophic vorticity is given by equation (3).

$$\zeta_g = \frac{1}{f\rho}\nabla^2 p + \frac{\beta}{f}u_g \tag{3}$$

$\beta = df/dy$, which is approximately 1.6 x 10^{-11} $s^{-1}m^{-1}$ at mid-latitudes. The magnitude of the second term on the right rarely exceeds 1 x 10^{-6} s^{-1}, a full order of magnitude less than

the second term on the right rarely exceeds 1 x 10^{-6} s^{-1}, a full order of magnitude less than

average vorticity values. Therefore, this term can be neglected and f can be treated as a local constant [*Carlson,* 1991], reducing equation (3) to:

$$\zeta_{gij} = \nabla^2 Q = (Q_{i+1,j} + Q_{i-1,j} - 2Q_{ij})/\Delta x^2 + (Q_{i,j+1} + Q_{i,j-1} - 2Q_{ij})/\Delta y^2 \qquad (4)$$

The initial guess for ζ_g is computed from the initial NCEP mean sea level pressure field on the 2.5° grid and then interpolated on the 0.25° domain grid. For each subsequent step the pressure fields and all calculations are on the 0.25° grid.

3.2 Variational Method

A variational method determines an optimal geostrophic stream function that smoothly blends NSCAT vorticity over the domain. The variational method minimizes the cost function (F) to find the solution fields Q_{ij} and ζ_{ij},

$$F(Q_{ij}, \zeta_{ij}, \lambda_{ij}) = \sum_i \sum_j \lambda_{ij}(\nabla^2 Q_{ij} - \zeta_{ij}) + \sum_i \sum_j \frac{K_\zeta}{2}(V_{ij})^2 + \sum_i \sum_j \frac{K_E}{2} G(Q_{ij}), \qquad (5)$$

where the terms on the right-hand side are summed over all the grid points i and j. The first term on the right-hand side is the model ($\zeta_g = \nabla^2 Q$), the unknown stream function and vorticity field, multiplied by a Lagrangian multiplier (λ_{ij}). This term is known as a "strong" constraint [*Saski,* 1970]. The second minimizes the data misfits (V_{ij}) between the new geostrophic vorticity (ζ_{ij}) and satellite vorticity, where available, and the misfits between the new and old geostrophic vorticity outside the swaths.

$$V_{ij} = \zeta_{ij} - K_S \zeta_{Sij}, \qquad \text{(in the swath)} \qquad (6)$$

$$V_{ij} = \zeta_{ij} - \zeta_{gij}, \qquad \text{(outside the swath)} \qquad (7)$$

$$V_{ij} = \zeta_{ij} - K_S \zeta_{Sij}, \qquad \text{(in the swath)} \qquad (6)$$

$$V_{ij} = \zeta_{ij} - \zeta_{gij}, \qquad \text{(outside the swath)} \qquad (7)$$

K_S is a coefficient needed to increase the NSCAT surface vorticity to geostrophic equivalent.

The NSCAT vorticity is a surface value, which before being blended with a geostrophic vorticity product, should be increased to a geostrophic equivalent. A simple method for relating geostrophic or gradient winds to surface winds uses reduction-rotation factors: geostrophic winds are multiplied by a constant of 0.6-0.9, depending on boundary layer stability, and rotated counterclockwise 15°-30° [*Clarke and Hess,* 1975]. *Harlan and O'Brien* [1986] used a least squares method to find an average reduction constant of 0.83 and rotation factor of 27.6° between geostrophic and Seasat-A winds. *Brown and Zeng* [1994] used their boundary layer model to arrive at a reduction constant of 0.667 and rotation factor of 18° for neutral stratification. Herein, K_S is chosen to be 1.5, the inverse of *Brown and Zeng's* reduction factor for neutral stability. The rotation factor is inconsequential, since rotating NSCAT winds by a constant angle has no effect on relative vorticity values.

The last term on the right of equation (4) is a penalty function that acts to smooth the solution field horizontally. Without this term the only solution is $\lambda = 0$, and satellite vorticity is substituted directly into the field. In general, the penalty function involves the second derivative of the solution field, often in the form of a Laplacian smoother. In this case, however, the Laplacian of Q is included in the model and another penalty function must be used. $G(Q_{ij})$ is chosen such that the kinematic geostrophic kinetic energy is minimized [*Harlan and O'Brien*, 1986].

$$G(Q_{ij}) = \frac{1}{2}(u_g^2 + v_g^2) = \frac{1}{2}\nabla Q \bullet \nabla Q \tag{8}$$

$$G(Q_{ij}) = \frac{1}{2}(u_g^2 + v_g^2) = \frac{1}{2}\nabla Q \bullet \nabla Q \tag{8}$$

The coefficients K_ζ and K_E are weights that control the balance between the amount of smoothing to be done and data misfits.

To arrive at the solution (Qij) the cost function must be minimized:

$$\frac{\partial F}{\partial Q_{ij}} = (\lambda_{i+1,j} + \lambda_{i-1,j} - 2\lambda_{ij})/\Delta x^2 + (\lambda_{i,j+1} + \lambda_{i,j-1} - 2\lambda_{i,j})/\Delta y^2$$
$$- \frac{K_E}{2}[(Q_{i+1,j} + Q_{i-1,j} - 2Q_{ij})/\Delta x^2 + (Q_{i,j+1} + Q_{i,j-1} - 2Q_{ij})/\Delta y^2] = 0 \qquad (9)$$

$$\frac{\partial F}{\partial \zeta_{ij}} = -\lambda_{ij} + K_\zeta V_{ij} = 0 \qquad (10)$$

$$\frac{\partial F}{\partial \lambda_{ij}} = \nabla^2 Q_{ij} - \zeta_{ij} = 0 \qquad (11)$$

Equation (9) can be written as

$$\nabla^2 \lambda_{ij} = \frac{K_E}{2} \nabla^2 Q_{ij} \ , \qquad (12)$$

and has a solution of the form

$$\lambda_{ij} = \frac{K_E}{2}(Q_{ij} - Q_{0ij}) \ , \qquad (13)$$

where Q_{0ij} is the homogeneous solution to $\nabla^2 \lambda_{ij} = 0$, and thus satisfies $\nabla^2 Q_{0ij} = 0$. On the boundaries $\lambda = 0$ and $Q_{0ij} = Q_{ij}$, therefore Q_{0ij} can be found through successive overrelaxation given the boundary values from the initial stream function field. Combining equations (10) and (13) and letting $K = K_E / K_\zeta$ leads to:

$$\zeta_{ij} = \zeta_{sij} + \frac{K}{2}(Q_{ij} - Q_{0ij}) \qquad \text{in the swath} \qquad (14)$$

$$\zeta_{ij} = \zeta_{gij} + \frac{K}{2}(Q_{ij} - Q_{0ij}) \qquad \text{outside the swath} \qquad (15)$$

Substituting (14) and (15) into (11) yields:

Substituting (14) and (15) into (11) yields:

$$(\Psi_{i+1,j} + \Psi_{i-1,j} - 2\Psi_{ij})/\Delta x^2 + (\Psi_{i,j+1} + \Psi_{i,j-1} - 2\Psi_{ij})/\Delta y^2 - \frac{K}{2}(\Psi_{ij} - \Psi_{0ij}) = \zeta_{sij}$$
in the swath (16)

$$(\Psi_{i+1,j} + \Psi_{i-1,j} - 2\Psi_{ij})/\Delta x^2 + (\Psi_{i,j+1} + \Psi_{i,j-1} - 2\Psi_{ij})/\Delta y^2 - \frac{K}{2}(\Psi_{ij} - \Psi_{0ij}) = \zeta_{gij}$$
outside the swath (17)

which are solved using successive overrelaxation and constant normal derivative boundary conditions.

Lagrangian multipliers (λ_{ij}) often have a physical interpretation. For example, by (10) the Lagrangian multipliers are the data misfits. Results show that their spatial distribution is dominated by small-scale noise, with variations at least one order of magnitude less than average vorticity values. No physical structures, such as the edges of the satellite swaths, are discernable in their distribution over the domain. The Lagrangian multipliers only correspond to grid-scale vorticity differences brought about by the smoothing term in the variational method.

As stated earlier, K is a coefficient that weights the relative contributions of the two constraints in the cost function. Furthermore, the two constraints are not dimensionally homogeneous and the coefficient must account for the difference in units in the two terms. A value of 1×10^{-13} m^{-2} produces a smooth pressure field while preserving the physical structures present in the NSCAT vorticity. Higher values put too much weight on minimizing the geostrophic kinetic energy, resulting in a pressure field with gradients that are too relaxed.

The geostrophic kinetic energy constraint does not, however, adequately filter out random noise present in the NSCAT vorticity. For this reason the solution stream field is horizontally smoothed once again with the following filter:

$$\Psi_{ij} = (\Psi_{i+1,j} + \Psi_{i-1,j} + \Psi_{i,j+1} + \Psi_{i,j-1} + 4\Psi_{ij})/8 \quad (18)$$

$$\Psi_{ij} = (\Psi_{i+1,j} + \Psi_{i-1,j} + \Psi_{i,j+1} + \Psi_{i,j-1} + 4\Psi_{ij})/8 \quad (18)$$

This filters out much of the real and artificial small scale variation in the vorticity field while

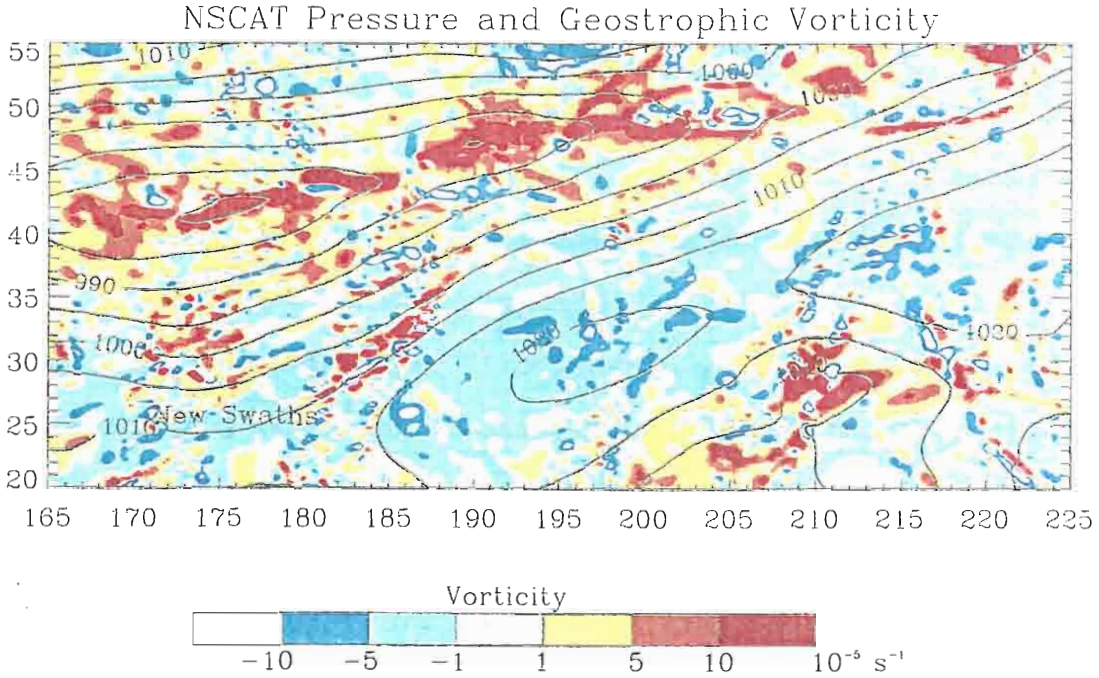

Figure 5. Surface pressure (mb) and geostrophic vorticity (s^{-1}) fields after assimilation of 22 passes of NSCAT (1800 UTC 5 January 1997). The two swaths from the last pass of the satellite are clearly visible on the left side of the domain, showing more noise in the vorticity due to less smoothing.

having minimal effect on an already smooth pressure field. Portions of the domain that undergo multiple iterations without any new satellite data are influenced by more passes of the filter than a portion with new data. This leaves more detail where new data are available, while blending away detail where the satellite data was last assimilated many iterations ago (figure 5). The weak constraint in the functional also acts to remove old information.

3.3 Boundary Conditions and Reference Pressures.

Solving equations (16) and (17) for Q_{ij} requires specification of boundary conditions on the borders of the domain. *Harlan and O'Brien* [1986] held the boundary pressure values constant, setting them equal to the values from NMC analyses. This condition is on the borders of the domain. *Harlan and O'Brien* [1986] held the boundary pressure values constant, setting them equal to the values from NMC analyses. This condition is

effective for their study, because the feature of interest is located in the center of the study area. In the interior of the domain, the solution field is loosely constrained by the boundary values, so their solution field realized the full influence of the assimilated scatterometer data over the low pressure system. Also, they assimilated satellite data only once for each NMC analysis, so their solution field was not required to evolve in time.

Constant normal derivative boundary conditions are used for this study. The gradient of the stream function normal to the boundary (based on the NCEP analysis) is computed at each grid point along the border. Equations (15) and (16) are then solved holding these normal derivatives constant. This approach allows the entire stream function field to evolve as NSCAT vorticity is assimilated, even near the boundaries. The drawback of using derivative boundary conditions is that the spatial mean pressure is not constrained: the mean can drift from the initial value in a manner other than the true temporal evolution of the mean. The horizontal gradients and relative highs and lows in the solution fields are realistic, but while assimilating one overpass the entire field can be displaced (between 0 and 6 mb) from ground truth. Without additional measures, this error adds up quickly as the procedure is repeated for additional satellite passes.

The drift in spatial mean pressure is remedied with reference pressures from within the domain. Ideally, the reference point(s) would be located near the center of the study area and away from sharp horizontal pressure gradients or extreme features. A constant offset could then be added or subtracted to the solution pressure field to make the solution and reference pressures equal. Unfortunately, buoys are only located in the domain by Hawaii and the Aleutians, near the southern and northern borders of the domain (Figure 3). The offset is taken as the average of the differences between the buoy pressure and the solution pressure at these points. Averaging minimizes the influence of locational errors in sharp gradients near the reference points.

gradients near the reference points.

The derivative boundary conditions still present limitations on the evolution of features

near the borders: Large scale features are not able to enter or leave the domain. For example, consider a low pressure system entering the domain on the western border. To correctly capture this feature as it crosses the border, the normal derivative of the pressure field should change from positive (increasing toward the interior) to negative. One way to accomplish this change is to update the boundary conditions with additional information. Based on domain size and the frequency with which new passes of the satellite occur, new derivative boundary conditions are computed from NCEP analyses every 24 hours. NCEP analyses are available every 6 hours, but updating boundary conditions every 6 or 12 hours made little difference in the evolution of the pressure fields. The weather systems in this study are sufficiently large and move slowly enough that their movement into and out of the domain can be resolved by updating the boundary conditions at 24 hour intervals. Using additional NCEP data to update the boundary conditions does not lessen the dependency of the solution field on NSCAT vorticity data. It simply provides a framework of large-scale horizontal pressure gradients to govern the solution near the borders.

3.4. Viability of the Technique

A major goal of this technique is to describe the evolution of cyclones based primarily on NSCAT observations. With the assimilation of data from each new pass of the satellite, less information is retained in the pressure field from the initial NCEP analysis. In 24 hours, 7 to 9 passes of the satellite over the domain cover around 75% of the area (Figure 3). In 48 hours the total is over 90% with a majority of the domain covered at least twice. At this point the geostrophic vorticity field is described almost exclusively by NSCAT vorticity. The pressure field follows from the geostrophic vorticity field, constrained only by the pressure field from the previous iteration, the derivative boundary conditions, and the two reference pressures. Continued assimilation of additional satellite passes changes

the two reference pressures. Continued assimilation of additional satellite passes changes the geostrophic vorticity field (and corresponding pressure field) as physical features move

and evolve in the domain. Ideally, this process continues throughout the life cycle of the feature of interest.

The technique does, however, have two limitations. First, the feature (cyclone, front) must have a strong signature in the satellite vorticity field. Results show that high values of relative vorticity ($> 1 \times 10^{-4}\ s^{-1}$) are concentrated at frontal zones and cyclone centers. If the feature is weak or diffuse, the noise and small scale variations in the NSCAT relative vorticity overwhelm the larger scale structure of the feature. The solution field diverges from the true pressure field, and this problem is compounded as more passes with weak signals are assimilated. Also, cells contaminated by attenuation from liquid water introduce error into the vorticity field. These errors do not appear to greatly affect the solution pressure fields for strong systems, as these errors are more local in nature and may not influence the large scale structure of the system. It is impossible, however, to determine the exact impact of the attenuation problem on the vorticity and pressure fields without knowing which cells are contaminated.

The technique also breaks down when the feature moves too quickly through the study area. Consider a cyclone moving west to east through the domain at 10 m/s. On the first day the satellite captures an area of high vorticity corresponding to center at a longitude of 175°E. This feature is assimilated into the pressure field and results in a low pressure center at that location. The satellite may not cover that location again in over 24 hours. Meanwhile, the true center of the cyclone would have moved nearly 800 km. If the satellite now captures the feature at its new location without updating the old location, the resulting vorticity and pressure fields will show the feature as an elongated area of low pressure. If the feature continues moving at a high speed, polar orbiting satellite coverage is insufficient to capture the movement of the cyclone properly and the solution field again diverges from the true pressure field.

to capture the movement of the cyclone properly and the solution field again diverges from the true pressure field.

CHAPTER 4

CASE STUDIES

4.1 Case 1: 18-24 December 1996

The method is first applied to a case of cyclogenesis that occurred 18-24 December 1996. The NCEP mean sea level pressure analysis from 0000 UTC 18 December 1996 initializes the process. The solution pressure field (hereafter called NSCAT pressure) evolves with the assimilation of data from 56 satellite passes over 7 days. Snapshots of the NSCAT pressure field are compared and contrasted with NCEP analyses made within three hours of the last satellite pass. Also, both the NSCAT and NCEP pressure fields are checked for consistency with the NSCAT wind vectors from the latest satellite pass. This comparison does not constitute validation of the NSCAT pressure fields, as an independent data source is necessary for objective results. It is simply intended to show how the NSCAT pressure fields conform to features seen in the NSCAT wind fields.

The first satellite pass covers only a small corner of the domain. The NSCAT pressure field changes very little from the NCEP initialization, aside from smoothing the discontinuities in the pressure field due to NCEP's 2.5 degree grid (Figure 6). This iteration demonstrates how the field retains the characteristics of the previous step over areas where no new satellite information is available for assimilation. After the assimilation of 8 passes, the NSCAT pressure field evolves considerably (Figure 7). The low pressure system near the northern border weakens (central pressure rises from 993 mb to 1002 mb) while the low near the southern border deepens in response to the strong vorticity values

system near the northern border weakens (central pressure rises from 993 mb to 1002 mb) while the low near the southern border deepens in response to the strong vorticity values

from the last satellite pass. The NCEP analysis from 1800 UTC 18 December 1996 does not intensify this system yet, showing a higher central pressure (1003 mb compared to 992 mb) and lower geostrophic vorticity values (less than 1 x 10^{-4} s^{-1}) than the NSCAT fields. Also, notice how the isobars tend to "kink" along features of high vorticity. Sharp bends in pressure contours are indicative of a sudden change in horizontal gradient, often associated with frontal zones (*Djuric'*, 1994).

On 1200 UTC 20 December 1996 the cyclone reaches its mature stage (Figure 8). The NSCAT central pressure is in good agreement with NCEP, both at 987 mb. NCEP appears to locate the center better, as the NSCAT wind vectors place the center of circulation at 39°N and 185°E, 1 degree east of the NCEP center. The NSCAT low pressure center is 5° south and 3° east of that location. The reason for this discrepancy stems from the strong vorticity between the two swaths of the latest satellite pass. This is older information (12-24 hours old) and has an impact on the NSCAT pressure field, causing somewhat of lag in the movement of the storm.

An interesting feature is the band of high vorticity at the bottom of the right swath. The change in direction of NSCAT wind vectors and the placement of this feature with respect to the circulation center suggests that it marks the trailing cold front. More will be said about the signature of fronts in NSCAT vorticity in Section 5.

By 1200 UTC 21 December 1996 the system weakens (Figure 9) to a central pressure of 995 mb (992 mb from NCEP). In the NSCAT pressure the low pressure center is located at 38°N and 188°E, coincident with the center of circulation of the NSCAT wind vectors. The NCEP center is offset 5° to the north and 4° to the east of the NSCAT position. The NCEP cyclone is now elongated along a major axis running northwest to southeast. The orientations of the NSCAT pressure contours, on the other hand, are more consistent with the wind vectors from the last satellite pass. The suspected front is still
southeast. The orientations of the NSCAT pressure contours, on the other hand, are more consistent with the wind vectors from the last satellite pass. The suspected front is still

apparent in the NSCAT vorticity field and has propagated 5° to the east.

Figure 10 shows the pressure fields at 1800 UTC 22 December 1996, after the assimilation of 39 satellite passes over 5 days. While the central pressures of the cyclone are similar, around 988 mb, the NSCAT and NCEP fields exhibit significant differences. The NCEP analysis builds high pressure in from the eastern boundary and sharpens the pressure gradient on the west side of the cyclone. This tendency is not seen in the NSCAT pressure field because there has been no new satellite data in this area for nearly 12 hours and the boundary conditions have not been updated in over 18 hours. The NSCAT field captures the feature once the satellite covers the west side of the domain on the next pass and the boundary conditions are updated (not shown). The NSCAT pressure field does, however, show improvements over NCEP on the east side of the domain due to the latest satellite pass. The front has pushed further eastward and is sharply delineated by a band of high vorticity values and a dramatic wind shift. The front is also resolved in the NSCAT pressure field, evidenced by the sharp kinks in the 1000 mb and 1005 mb isobars. NCEP either misplaces the front (the kink in the 995 mb contour is 5° too far north), or does not resolve them.

Two days later on 1200 UTC 24 December 1996 the cyclone reintensifies with a central pressure of 979 mb (Figure 11). The storm is large, nearly covering the entire domain. NSCAT and NCEP are in good agreement with both the location and pressure of the center. Both fields are also consistent with the NSCAT wind vectors. A frontal zone now extends eastward from the cyclone's center. The NSCAT pressure field resolves this feature sharply as seen in the kinks in the 995 mb and 1000 mb contours and strong pressure gradients normal to the front. The NCEP analysis has gently curving contours in this zone, making the exact location of the front difficult to determine. On the western border NCEP has a small area of low pressure and strong geostrophic vorticity (centered at

border NCEP has a small area of low pressure and strong geostrophic vorticity (centered at
32°N and 167°E) which the NSCAT field totally misses. The low is a fast-moving feature

that entered the domain after the last pass of the satellite over the area.

4.2. Case 2: 3-6 January 1997

This is a case of frontogenesis that took place during 3-6 January 1997. The process is initialized at 0000 UTC 3 January 1997, when the only feature of interest is a weak low pressure system centered at 48°N and 177°E (Figure 12). The NSCAT field picks up another low pressure lobe entering the domain on the western border at 40°N, while this feature is not seen in the NCEP pressure field.

The next snapshot is at 1800 UTC 3 January 1997 (Figure 13). The low moves east and, according to the NSCAT pressure field, is centered at 50°N and 190°E with a central pressure of 994 mb. The NCEP analysis places the center 2° south and east of the NSCAT location with a central pressure of 987 mb. The NSCAT low pressure center location exactly matches the center of circulation of the wind vectors. NSCAT also does a better job of showing the elongated nature of the low, especially on the eastern end. Notice how the wind vectors parallel the NSCAT contours in this area. NCEP does not extend the low far enough east, as the wind vectors cross the contours at unrealistically large angles, flowing from low to high pressure.

The low moves little in the next 18 hours. The center is now located at 49°N and 191°E in the NSCAT pressure field (Figure 14), coincident with the center of circulation as defined by the wind vectors. NCEP continues to place the center too far to the east by 3°. The NCEP central pressure is 982 mb, 7 mb less than the NSCAT value. The NCEP analysis places another distinct low at 42°N and 176°E, where the NSCAT field has a more continuous trough extending east to west across the northern portion of the domain. NSCAT wind vectors do not suggest a closed circulation around NCEP's secondary low, so the NSCAT pressure field is likely more realistic. The NSCAT low pressure system is stretched longitudinally, becoming more of a linear trough than an organized cyclone.

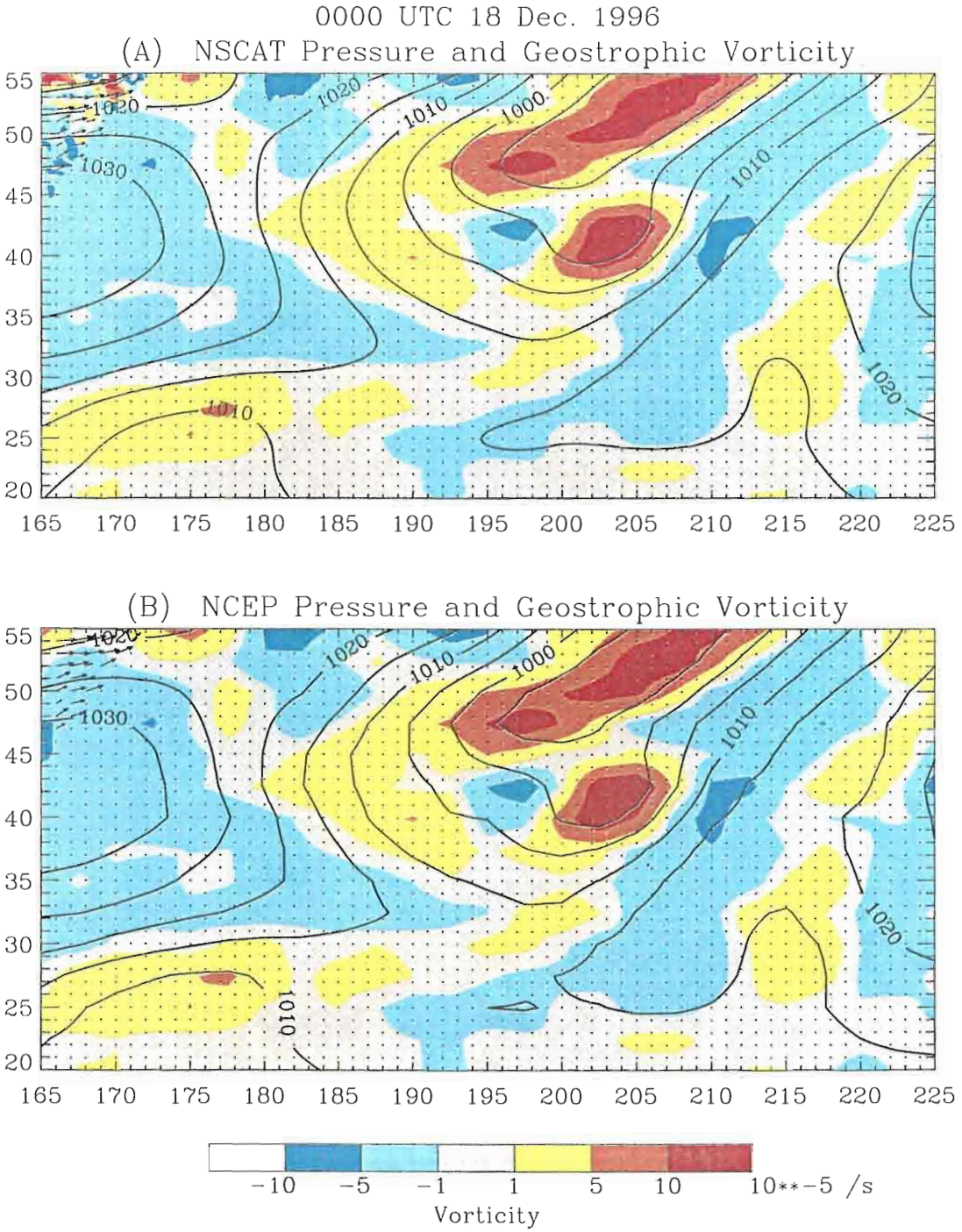

Figure 6. Surface pressure (mb) field and geostrophic vorticity (s^{-1}) for (A) NSCAT solution and (B) NCEP reanalysis on 0000 UTC 18 December 1996. Vectors show relative NSCAT winds from the latest

Figure 6. Surface pressure (mb) field and geostrophic vorticity (s^{-1}) for (A) NSCAT solution and (B) NCEP reanalysis on 0000 UTC 18 December 1996. Vectors show relative NSCAT winds from the latest
satellite pass.

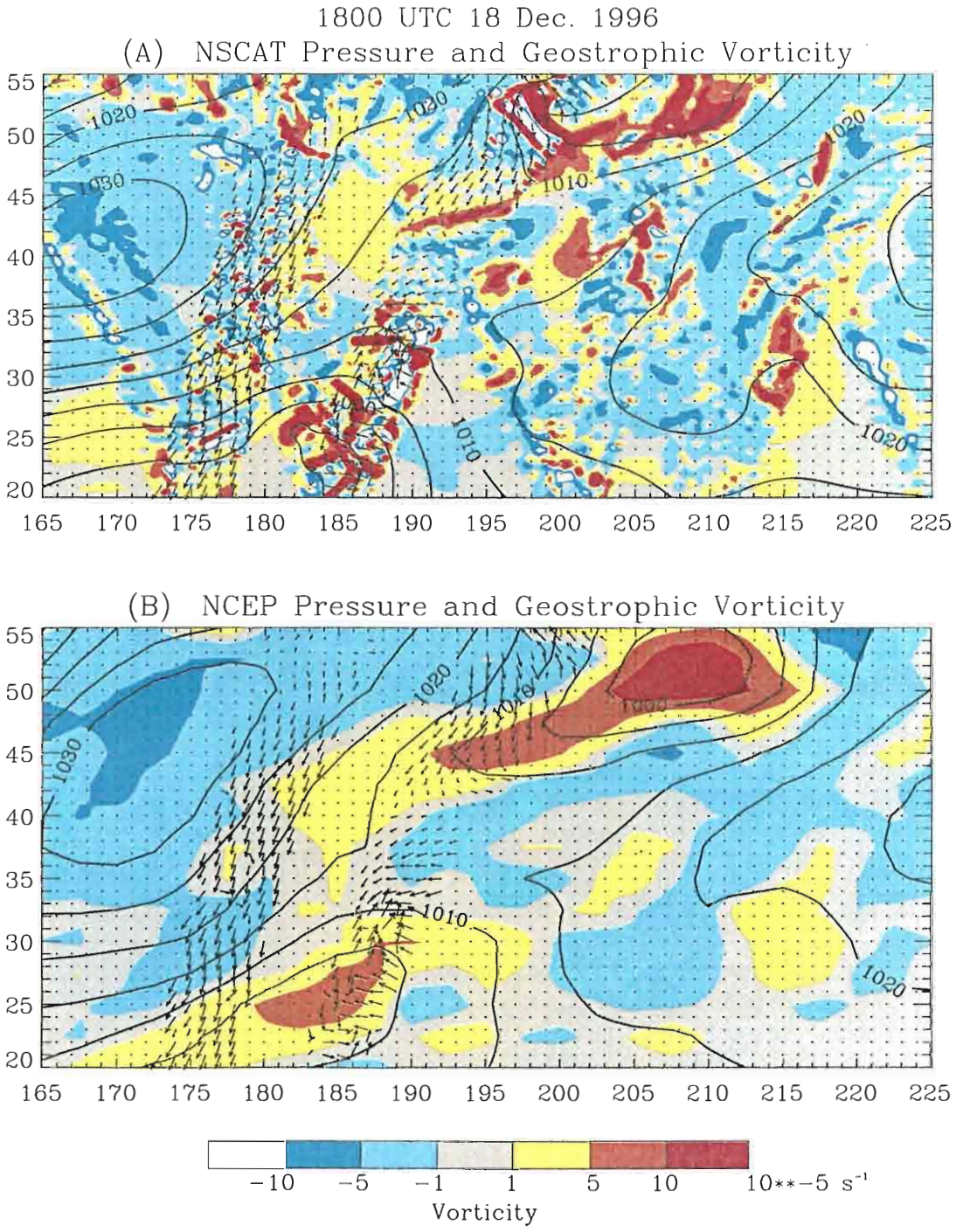

Figure 7. Same as figure 6 for 1800 UTC December 1996. Low pressure centered near 22°N and 185°E intensifies, and is deeper than in the NCEP field.

Figure 7. Same as figure 6 for 1800 UTC December 1996. Low pressure centered near 22°N and 185°E intensifies, and is deeper than in the NCEP field.

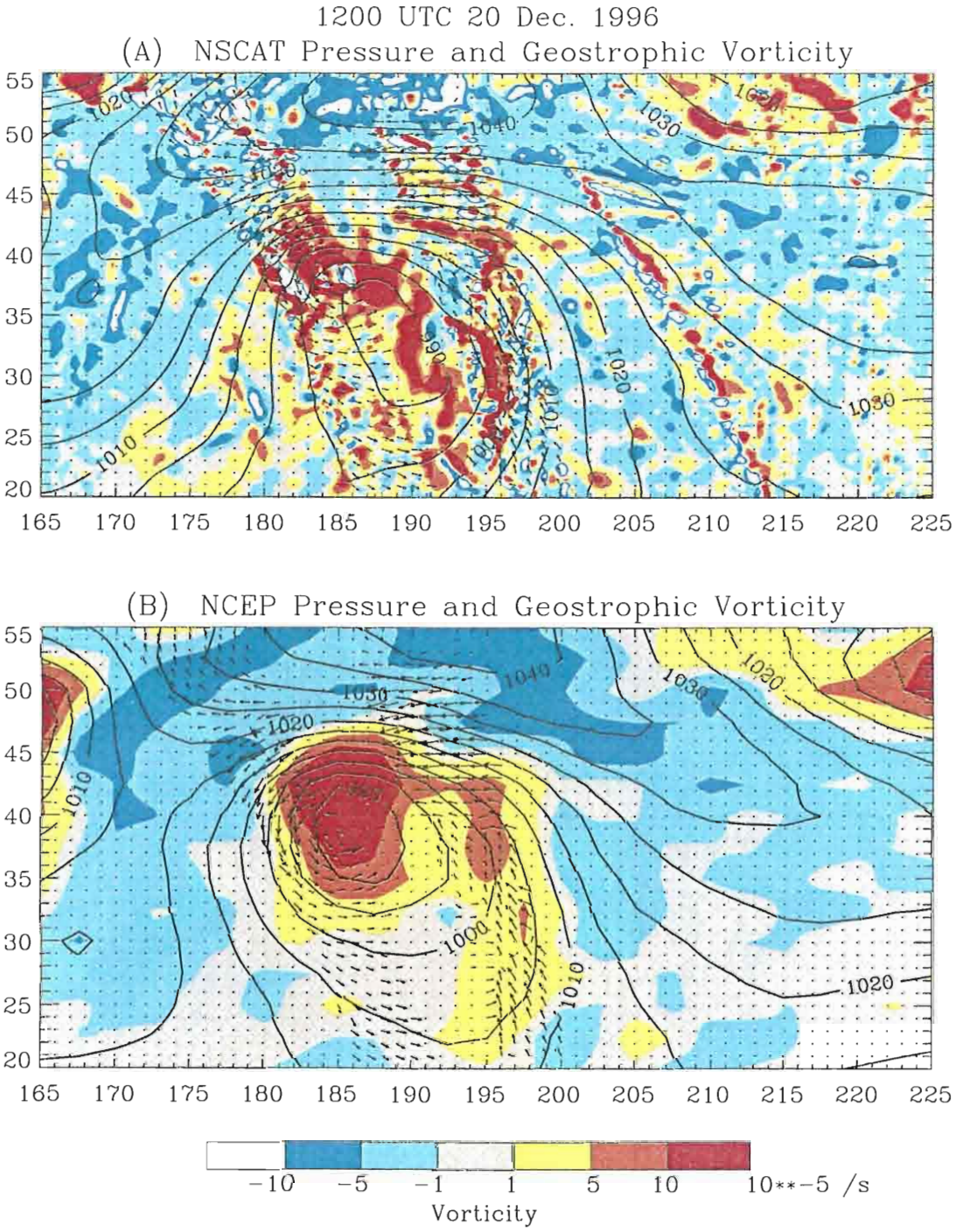

Figure 8. Same as figure 6 for 1200 UTC 20 December 1996. Mature cyclone and trailing cold front.

Figure 8. Same as figure 6 for 1200 UTC 20 December 1996. Mature cyclone and trailing cold front.

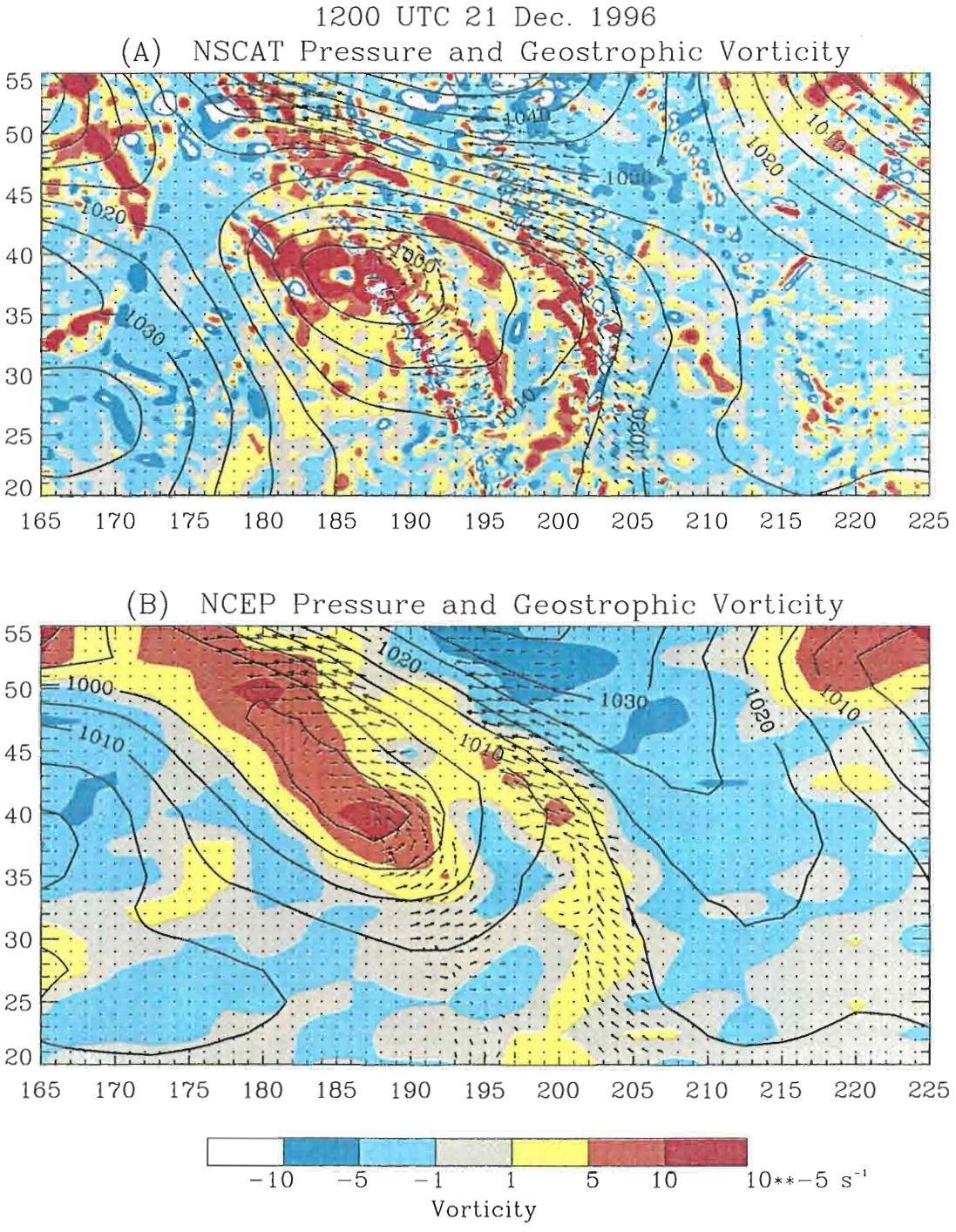

Figure 9. Same as figure 6 for 1200 UTC 21 December 1996. Note the difference in structure and location of the cyclone in the two analyses.

Figure 9. Same as figure 6 for 1200 UTC 21 December 1996. Note the difference in structure and location of the cyclone in the two analyses. NSCAT winds are more consistent with the NSCAT pressure field.

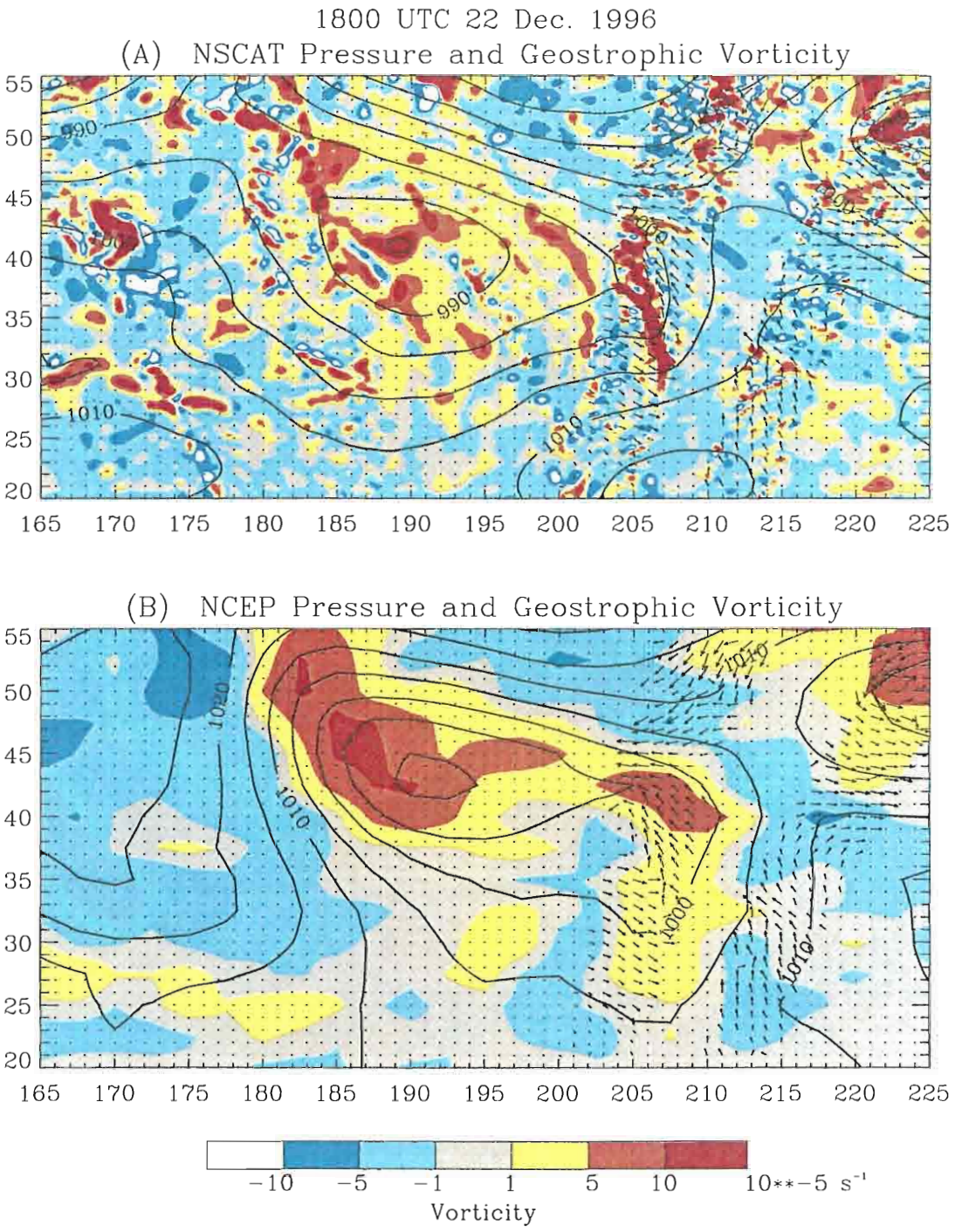

Figure 10. Same as figure 6 for 1800 UTC 22 December 1996. The cold front has propagated east and is now seen in the NSCAT pressure field. NCEP

Figure 10. Same as figure 6 for 1800 UTC 22 December 1996. The cold front has propagated east and is now seen in the NSCAT pressure field. NCEP has problems placing this feature.

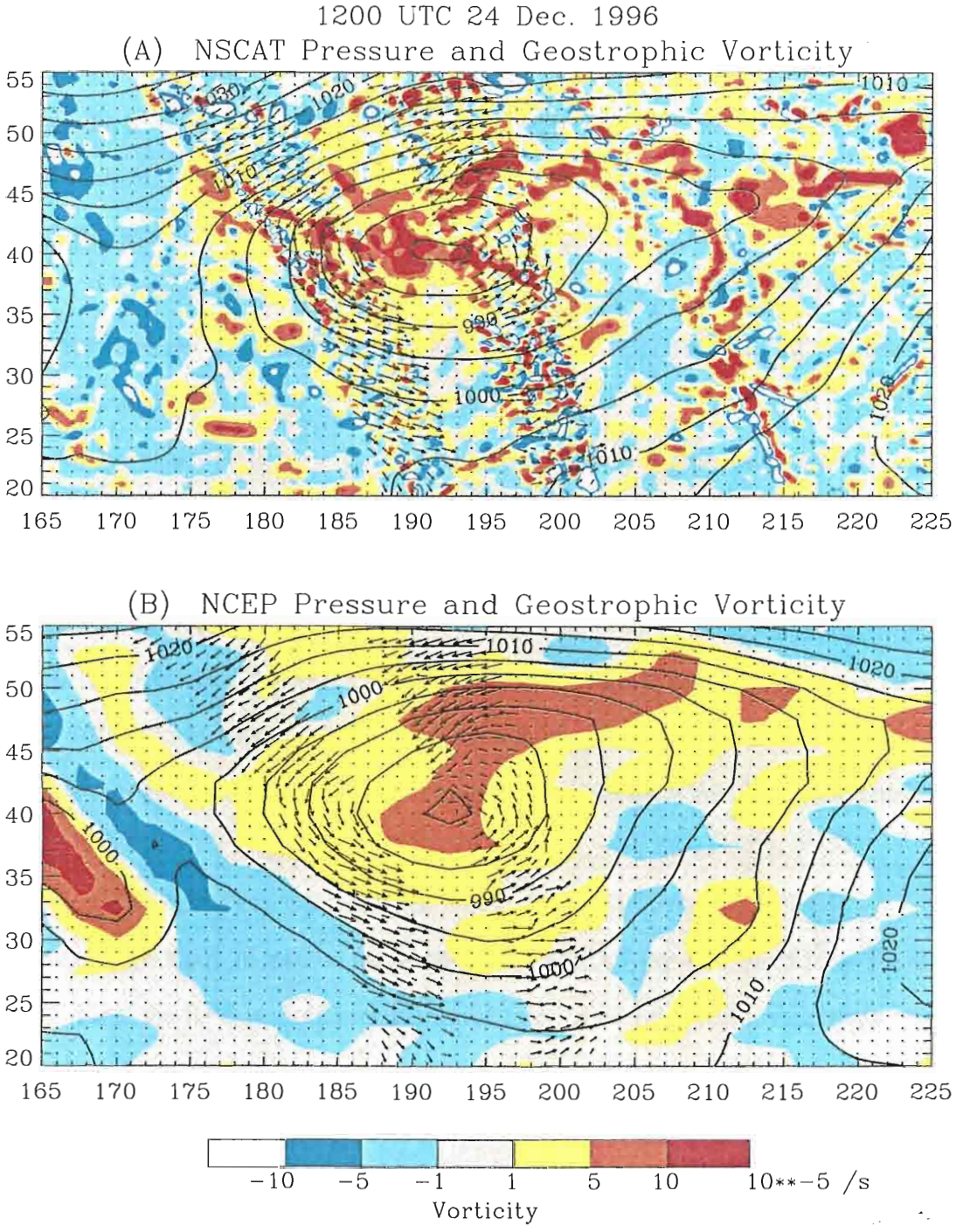

Figure 11. Same as figure 6 for 1200 UTC 24 December 1996. The cyclone reintensifies and the NSCAT analysis forms a new frontal feature extending

Figure 11. Same as figure 6 for 1200 UTC 24 December 1996. The cyclone reintensifies and the NSCAT analysis forms a new frontal feature extending
east from the center.

Six hours later, at 1800 UTC 4 January 1997, an apparent front has formed and extends across the northern portion of the study area (Figure 15). The front in the NSCAT pressure field is defined by a nearly continuous band of high vorticity and low pressure. North of the front the winds are east-northeast, while south of the front they are from the west-southwest. Also, pressure gradients have tightened on both sides of the front. The wind shift line coincides well with location of the high vorticity band and lowest pressures. The NCEP analysis persists in separating the feature into two different lows. NSCAT wind vectors show no evidence of closed circulation around either of the features to support this analysis.

The front is nearly stationary for the next 24 hours and is sharply delineated by the 1800 UTC 5 January 1997 NSCAT pressure and vorticity fields (Figure 16). The wind shift across the front from northeast to west and southwest is highly localized along the length of the front. NCEP finally merges the two lows into one elongated feature, although it is not as linear as depicted by the NSCAT field. The NSCAT field has lower pressure (979 mb) than NCEP (988 mb) on the western portion of the front. Otherwise, the positions of two small low pressure features along the front agree well with the wind circulation patterns.

4.3 Accuracy of the NSCAT and NCEP Pressure Fields.

Two generalizations can be made about the NSCAT pressure field from these case studies. First, the field is more realistic in the interior of the domain rather than near the boundaries. New features moving into the domain are not assimilated into the NSCAT pressure field until the satellite passes over the area, so these features may be totally missed. Also, the orientation of contours near the borders may not be correct because the NSCAT field has no information on the shape of features outside the domain. For example, the low in the northeast corner of the domain in Figures 8 and 9 is depicted by NCEP as a small, weak lobe running west to east and out of the domain. The NSCAT

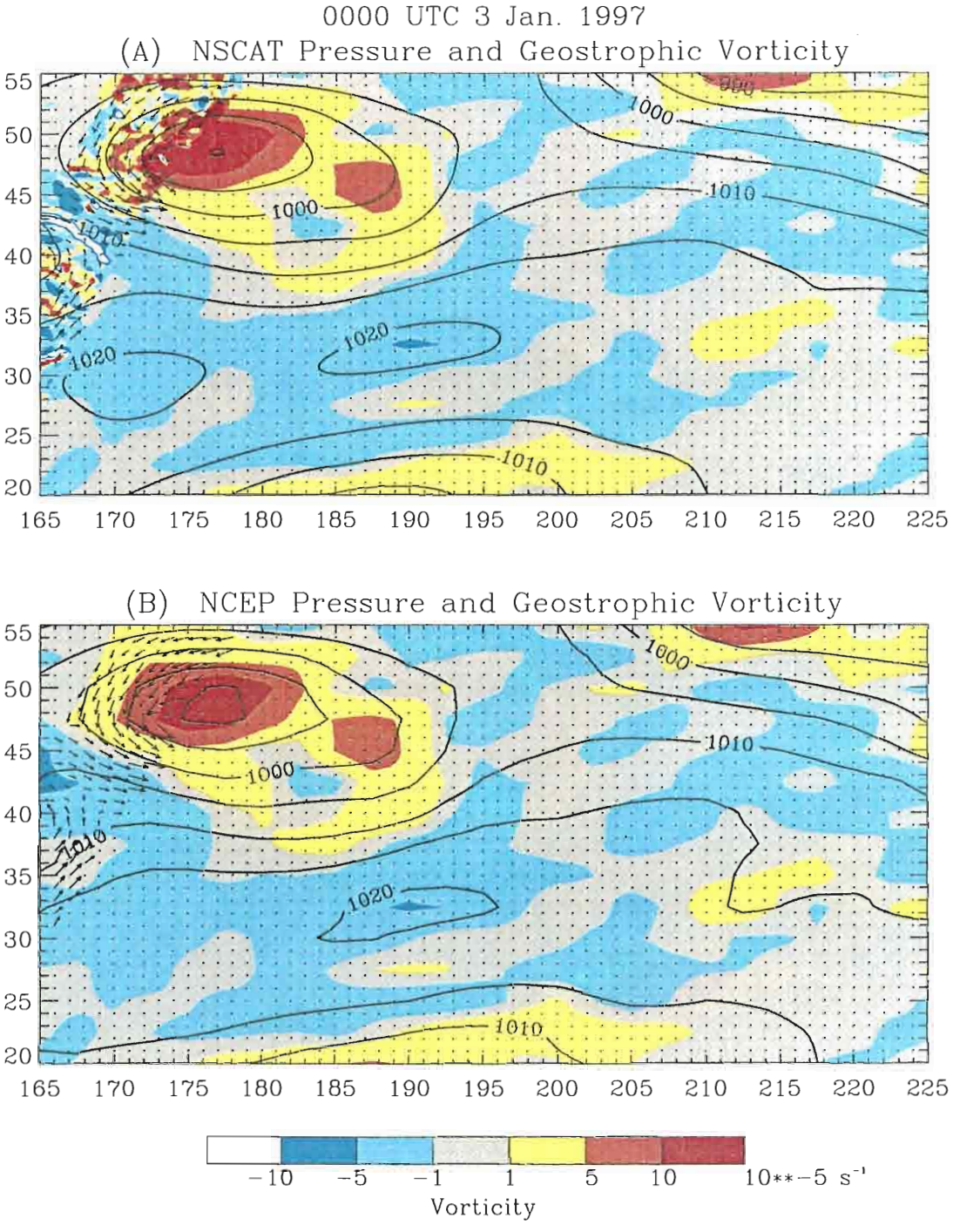

Figure 12. Same as figure 6 for 0000 UTC 3 January 1997. NCEP analysis used to initialize Case 2 and NSCAT pressure field after the assimilation of

Figure 12. Same as figure 6 for 0000 UTC 3 January 1997. NCEP analysis used to initialize Case 2 and NSCAT pressure field after the assimilation of
one swath.

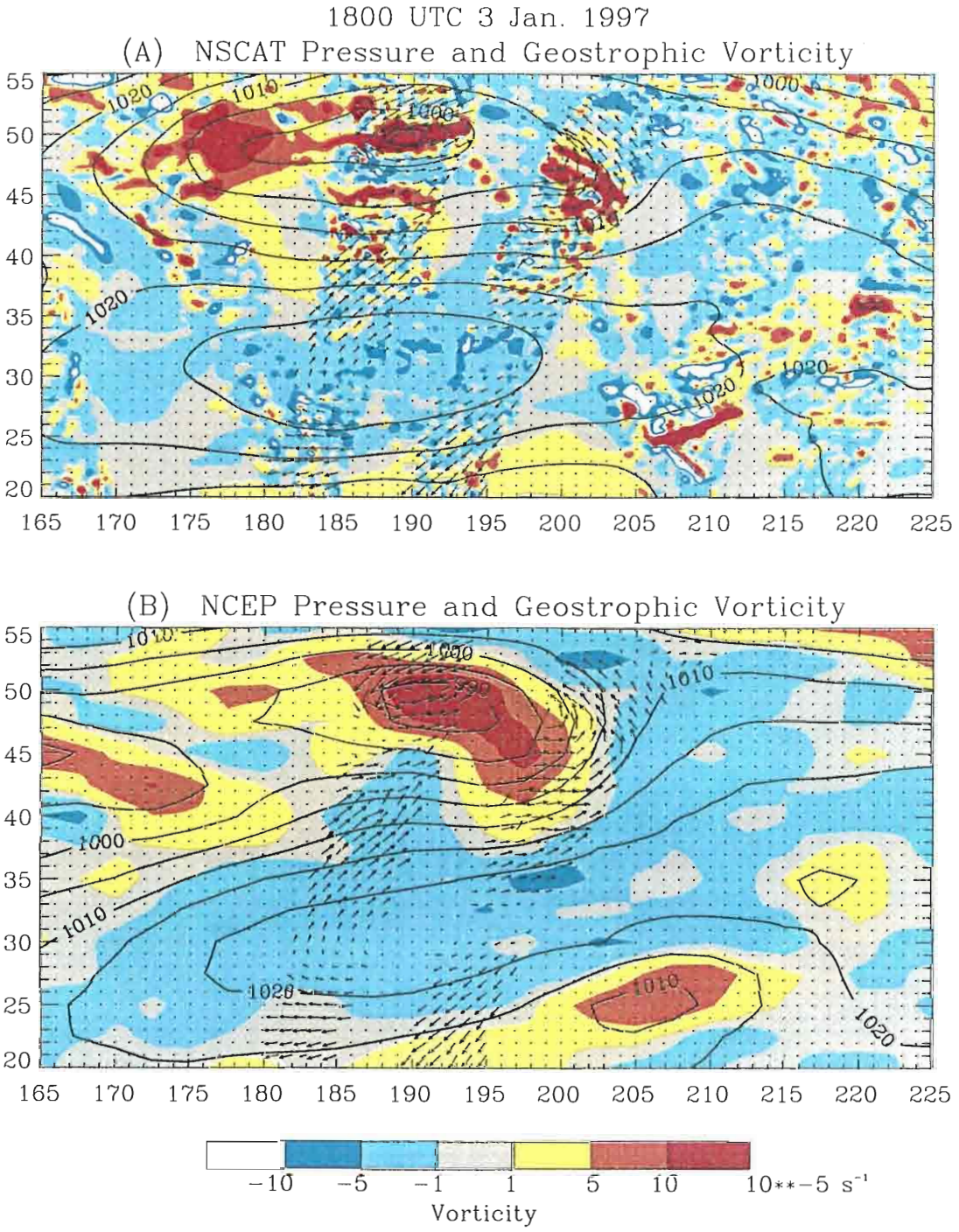

Figure 13. Same as figure 6 for 1800 UTC 3 January 1997. NSCAT low pressure center location and eastern lobe are more consistent with NSCAT

Figure 13. Same as figure 6 for 1800 UTC 3 January 1997. NSCAT low pressure center location and eastern lobe are more consistent with NSCAT winds.

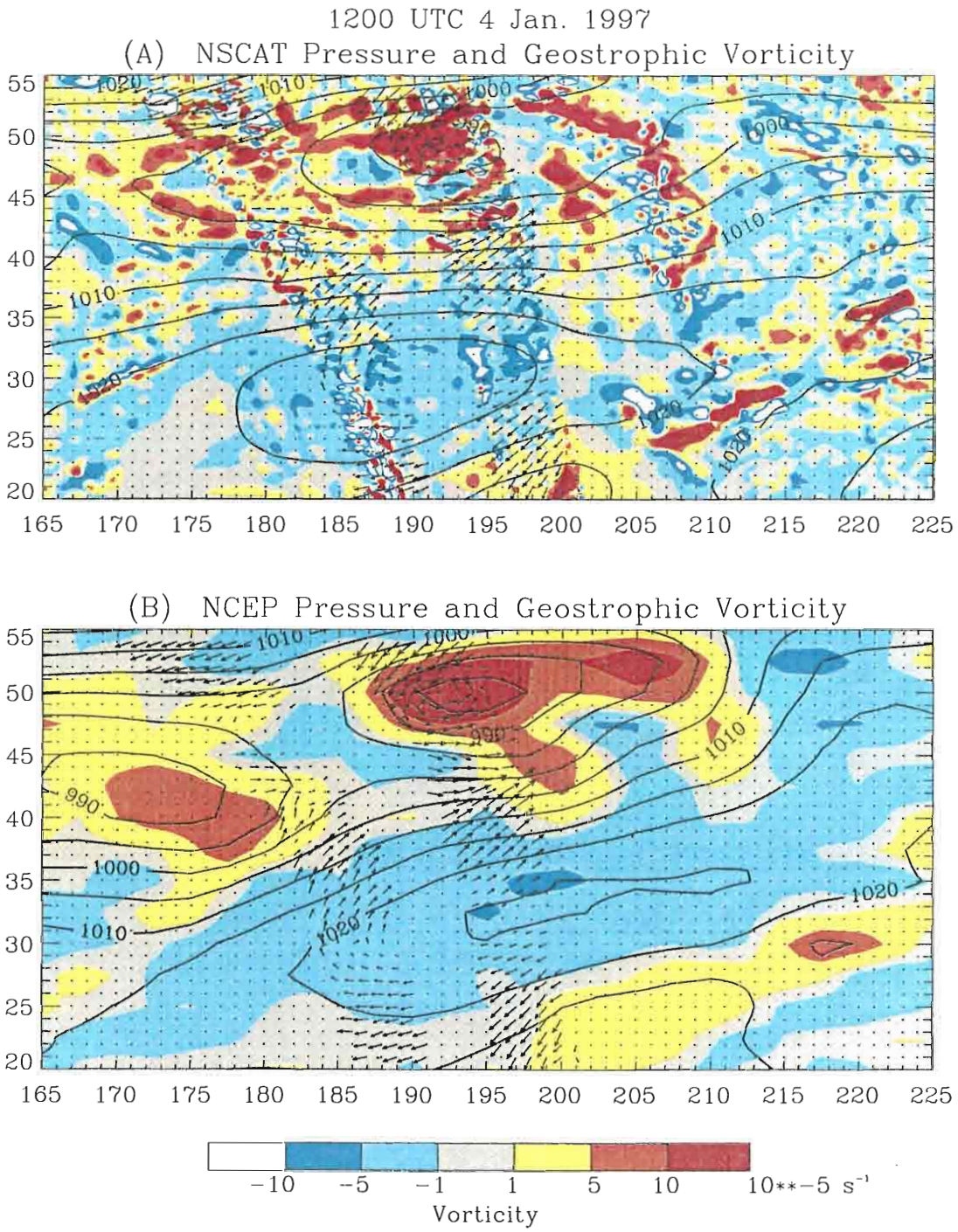

Figure 14. Same as figure 6 for 1200 UTC 4 January 1997. NSCAT shows elongated trough while NCEP has two separate low pressure centers.

Figure 14. Same as figure 6 for 1200 UTC 4 January 1997. NSCAT shows elongated trough while NCEP has two separate low pressure centers.

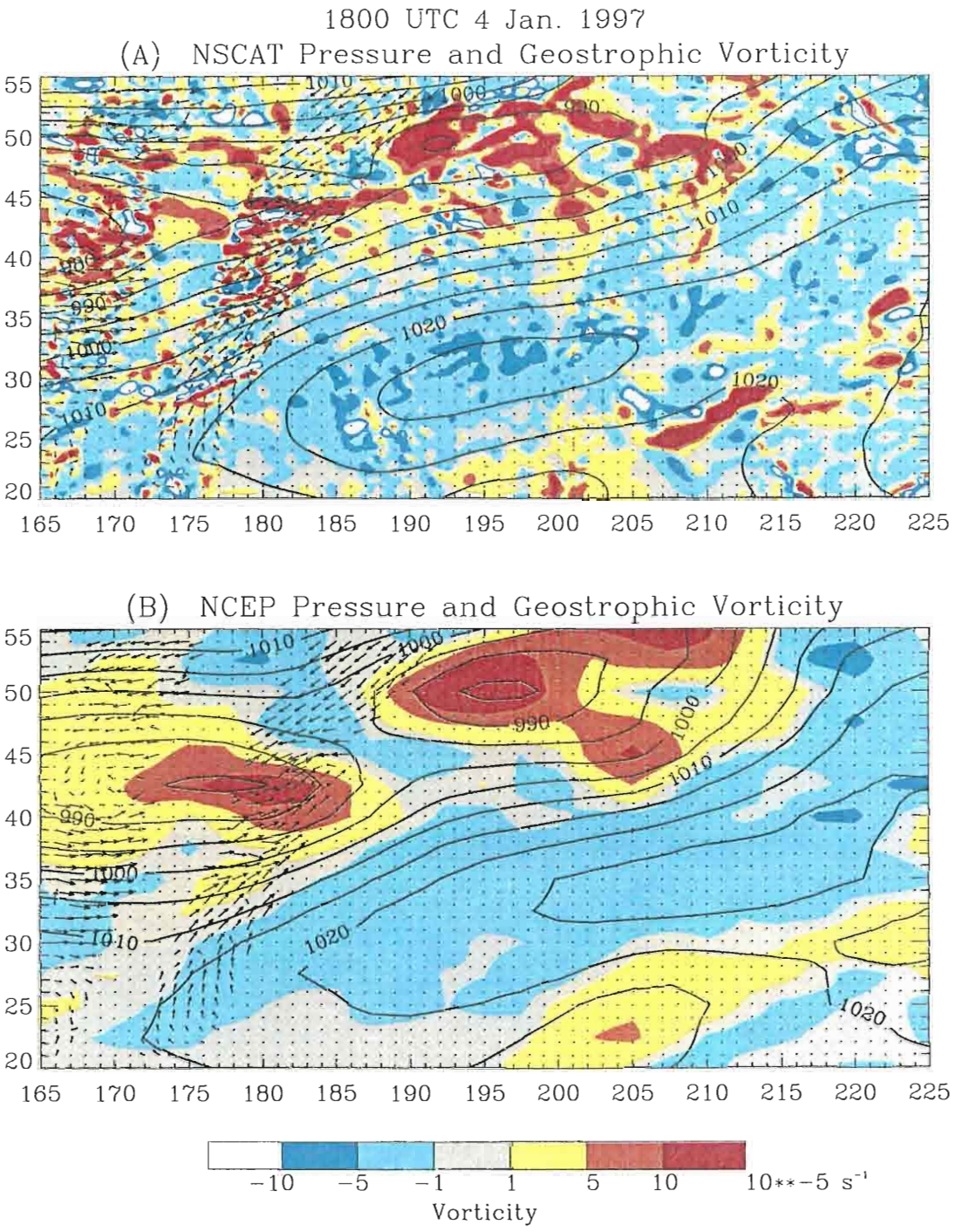

Figure 15. Same as figure 6 for 2800 UTC 4 January 1997. Feature is more frontal than cyclonic. NCEP still has two separate lows.

Figure 15. Same as figure 6 for 2800 UTC 4 January 1997. Feature is more frontal than cyclonic. NCEP still has two separate lows.

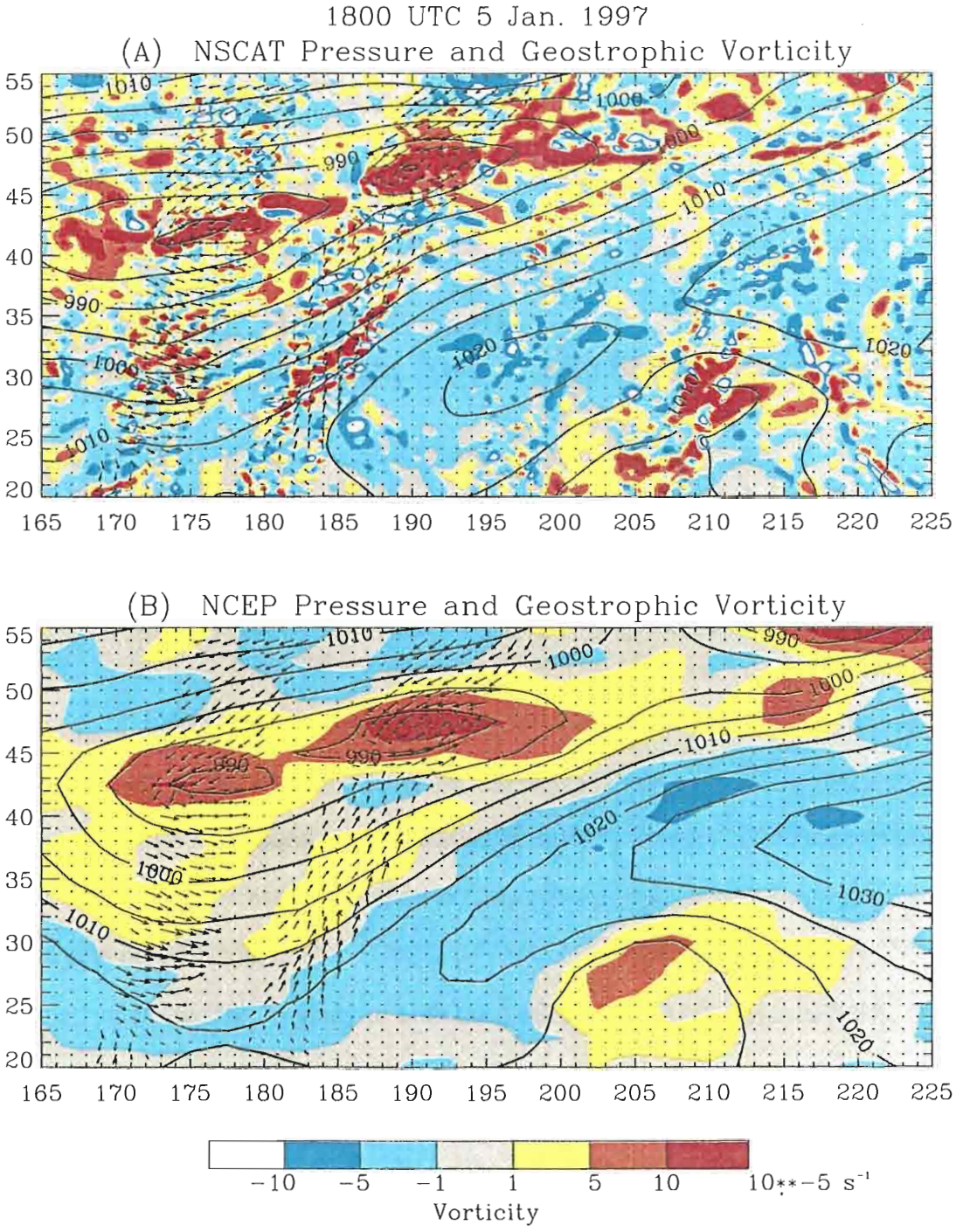

Figure 16. Same as figure 6 for 1800 UTC 5 January 1997. Well defined front stretches across the northern portion of the domain.

Figure 16. Same as figure 6 for 1800 UTC 5 January 1997. Well defined front stretches across the northern portion of the domain.

Table 1. Comparison with Surface Data

Time and Date	NSCAT interior		NSCAT near swath		NSCAT near swath and buoy		NCEP interior	
	Mean diff. (mb)	Std. Dev. (mb)	Mean diff. (mb)	Std. Dev. (mb)	Mean diff. (mb)	Std. Dev. (mb)	Mean diff. (mb)	Std. Dev. (mb)
1800 UTC 18 Dec.	1.6	3.8	-0.8	3.3	2.6	2.6	-0.2	1.7
1200 UTC 20 Dec.	4.3	7.0	2.2	8.5	0.3	5.8	0.2	4.2
1200 UTC 21 Dec.	4.6	6.2	4.5	6.8	4.4	4.7	0.6	3.2
1800 UTC 22 Dec.	-5.2	8.2	0.5	2.8	0.7	1.4	-0.1	1.4
1200 UTC 24 Dec.	-0.5	3.0	0.7	1.9	Insuff.	data	0.4	3.2
1800 UTC 3 Jan.	3.6	7.2	4.4	3.2	1.5	2.3	1.2	5.8
1200 UTC 4 Jan.	-0.4	7.8	1.8	6.3	1.7	2.4	0.2	4.7
1800 UTC 4 Jan.	-2.5	4.9	-3.8	4.8	Insuff.	data	0.0	4.3
1200 UTC 5 Jan.	-3.9	5.1	-5.8	3.8	2.2	1.6	-0.2	5.1

pressure field, however, aligns the contours as if a strong, large low pressure system is located northeast of the domain. Secondly, the NSCAT pressure field is more accurate where the satellite has passed more recently. It stands to reason that the portion of the domain updated with newer information is more current than an area than has not seen a satellite pass in many hours.

Table 1 addresses the accuracy of both the NSCAT and NCEP pressure fields. Three hourly surface pressure observations from ships and buoys (courtesy of the National Climate Data Center) are compared to values from both the NSCAT and NCEP pressure fields for each snapshot in figures 6-11 and 13-16. For each case the mean and standard deviation of the difference of the pressure field values and the *in situ* observations are computed using all available *in situ* observations at that time. These statistics are computed
deviation of the difference of the pressure field values and the *in situ* observations are computed using all available *in situ* observations at that time. These statistics are computed

for (A) all observations in the interior of the domain (at least 5° from the boundaries), (B) observations within 200 km of the last satellite swaths, and (C) observations within 200 km of the last satellite swaths and within 1,000 km of the reference buoys. Condition (C) had to be extended to 1,000 km from the reference buoys in order to include a meaningful number of observations (> 5). Even at this distance two of the cases had an insufficient number of observations to compute statistics for condition (C). The NCEP statistics are computed for condition (A).

The results from the interior of the domain show that the NCEP pressure field is quantitatively more accurate than the NSCAT field over the domain as a whole. The NSCAT mean difference ranges from 0.5 to 5.2 mb in magnitude and the standard deviation is between 3.0 and 8.2 mb. The NCEP mean difference is small, between 0.1 and 1.2 mb and the standard deviation is less than or equal to 5.8 mb. NCEP should be more accurate for several reasons. First, the observations were made at the same synoptic times as the NCEP analyses. The NSCAT field, however, may have seen the last satellite pass as far as ± 3 hours of the synoptic time. Also, the NSCAT pressure field outside the area covered by the latest pass is based on older satellite vorticity values, 12 to 24 hours from the latest pass. Yet another source for error in the NSCAT field is the sparsity of reference pressures. Only two buoys were available in the domain, and these are both located in the eastern half of the area. Inaccuracies in the pressure gradients caused by older satellite vorticity lead to increasing errors with distance from the reference points.

Results from the comparison of the NSCAT field to only those observations near the latest swaths show, with two minor exceptions, decreases in the mean difference. The standard deviation also decreases for all cases except 1200 UTC 20 December 1996. One outlier within the swath is responsible for this increase due to the decreased number of samples. These results support the assertion that the NSCAT pressure field is more

samples. These results support the assertion that the NSCAT pressure field is more
accurate near the latest swaths.

Table 2: Difference in the Locations of Low Pressure Centers Compared to Centers of Circulation

Date and Time	NSCAT			NCEP		
	Lat. (°)	Lon. (°)	Distance (km)	Lat. (°)	Lon. (°)	Distance (km)
1200 20 Dec.	-5.0	4.0	650	0.0	2.0	315
1800 20 Dec.	0.0	0.0	0	1.0	1.0	135
1200 21 Dec.	0.0	1.0	80	-3.0	3.0	400
1200 22 Dec.	-1.0	1.0	135	5.0	3.0	600
1800 22 Dec.	-2.0	0.0	225	0.0	0.0	0
1200 23 Dec.	0.0	2.0	315	0.0	2.0	315
1800 23 Dec.	0.0	0.0	0	0.0	0.0	0
1200 24 Dec.	0.0	0.0	0	0.0	0.0	0
1800 3 Jan.	0.0	-1.0	80	-1.0	2.0	200
1200 4 Jan.	0.0	0.0	0	0.0	2.0	315
Average	-0.8	0.7	150	0.2	1.5	230

Comparisons of the NSCAT pressure to only those surface observations near the latest swaths and also near the reference buoys exhibit further decreases in the mean difference for the cases where the mean difference was relatively high in the previous comparison (> 4.4 mb). The standard deviation decreases in all cases and is less than the NCEP standard deviation in 7 out of the 9 cases, proving the NSCAT pressure field is quite accurate near the latest swath and near the reference points. Incorporating more reference points into the solution of the NSCAT pressure field should have a beneficial effect on the accuracy of the field as a whole.

Although the NSCAT pressures may not be quantitatively more accurate than NCEP over the domain as a whole, the qualitative advantages are seen in the detailed comparisons made in sections 4.1 and 4.2. Features such as fronts are more sharply defined and

over the domain as a whole, the qualitative advantages are seen in the detailed comparisons made in sections 4.1 and 4.2. Features such as fronts are more sharply defined and pressure gradients are more consistent with the NSCAT winds. The improved detail in the

geostrophic vorticity fields gives rise to features in the NSCAT pressure fields that are blurred or not seen at all in the NCEP analyses.

NSCAT also is better at placing the low pressure centers correctly with respect to the center of circulation of the NSCAT winds. Again, and independent data source would lead to a more objective comparison, but the lack of conventional data over the North Pacific makes the NSCAT wind vectors the best alternative for determining correct location of low pressure centers. Table 2 shows the difference in location of low pressure centers compared to circulation centers for times when the circulation center is revealed in the latest satellite path. In two of the ten cases both NSCAT and NCEP agree exactly with the NSCAT winds. In the first case, at 1200 UTC 20 December 1996, NSCAT differs significantly from the center of circulation because an older vorticity maximum lies between the two swaths of a newer pass, giving a false vorticity signature to the new NSCAT pressure field (see section 4.1). Other than this isolated case, NSCAT pressure fields are consistently closer to the circulation center than NCEP. On average, NSCAT low pressure centers are 150 km from the center of circulation and NCEP centers are 230 km away. An interesting feature of table 2 is the trend in longitudinal error of the NCEP low pressure centers. In 7 out of the ten cases the NCEP center is placed too far eastward when compared to circulation centers; the center is misplaced to the west in none of the cases. While 10 cases are too few to suggest a systematic bias in the NCEP analyses, the trend warrants further investigation.

CHAPTER 5

FRONTAL DETECTION

A secondary of this study deals with the strong signature of surface fronts in the relative vorticity field computed from NSCAT winds. The identification and location of fronts using satellite remote sensing has long been a topic of great interest. Visible and IR imagery has taught us a great deal about the structure and evolution of extratropical cyclones [*Carlson,* 1980; *Browning and Roberts,* 1992]. This type of imagery, however, has one inherent drawback. Broad cloud cover at higher levels obscures features at lower levels and at the surface. Only in well organized, sharply-defined systems can the approximate location of surface fronts be determined from such passive sensors. *Katsaros et al.,* [1996] used parameters from active/passive microwave sensors aboard SSM/I, Geosat, and ERS-1 satellites to study the evolution of marine cyclones. They found that frontal zones could be identified by large gradients in the SSM/I integrated water vapor. Unfortunately, this parameter is a measure of water vapor over the entire atmospheric column and cannot isolate features at the surface. The location of fronts changes with height because of the sloped surface of the air mass. Consequently, the integrated water vapor can only identify a broad frontal zone representative of many levels rather than a sharp line at the surface. *Katsaros et al* [1996] also used Geosat and ERS-1 altimeter wind speeds to identify wind speed gradients in the vicinity of fronts. These altimeter data were often obscured by precipitation in the area of interest, especially in the frontal zones.

Surface fronts can be identified in NSCAT winds by changes in wind speed and

were often obscured by precipitation in the area of interest, especially in the frontal zones.

Surface fronts can be identified in NSCAT winds by changes in wind speed and

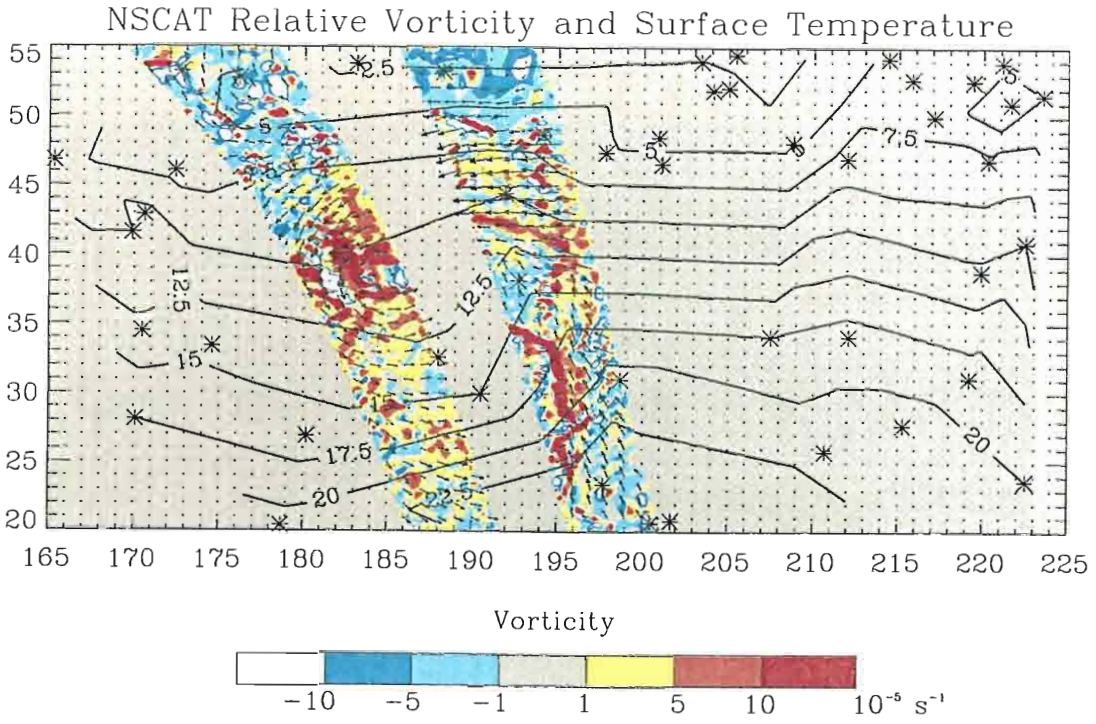

Figure 17. NSCAT winds and relative vorticity from a single satellite pass at 1800 UTC 20 December, 1996. Isotherms (°C) are from NCDC ship and buoy data (asterisks mark individual observations). A cold front is identified by the band of high relative vorticity near the bottom of the right swath.

direction. These changes are often subtle, though, making the exact location of a front difficult to determine by visual examination of wind fields. When relative vorticity is computed from NSCAT winds, however, even subtle changes in wind speed and direction lead to large values of relative vorticity ($> 1 \times 10^{-4}$ s^{-1}). Fronts are characterized by relatively low pressure at the boundary where air masses of higher pressure meet. Winds curve counterclockwise in response to the localized pressure minimum, resulting in high positive relative vorticity values (in the northern hemisphere).

Plots of relative vorticity in the NSCAT swaths are presented showing linear bands of high relative vorticity near surface fronts. Figure 17 plots the dual swaths of NSCAT winds and relative vorticity over a mature cyclone at 1200 UTC 20 December 1996 (same

high relative vorticity near surface fronts. Figure 17 plots the dual swaths of NSCAT winds and relative vorticity over a mature cyclone at 1200 UTC 20 December 1996 (same

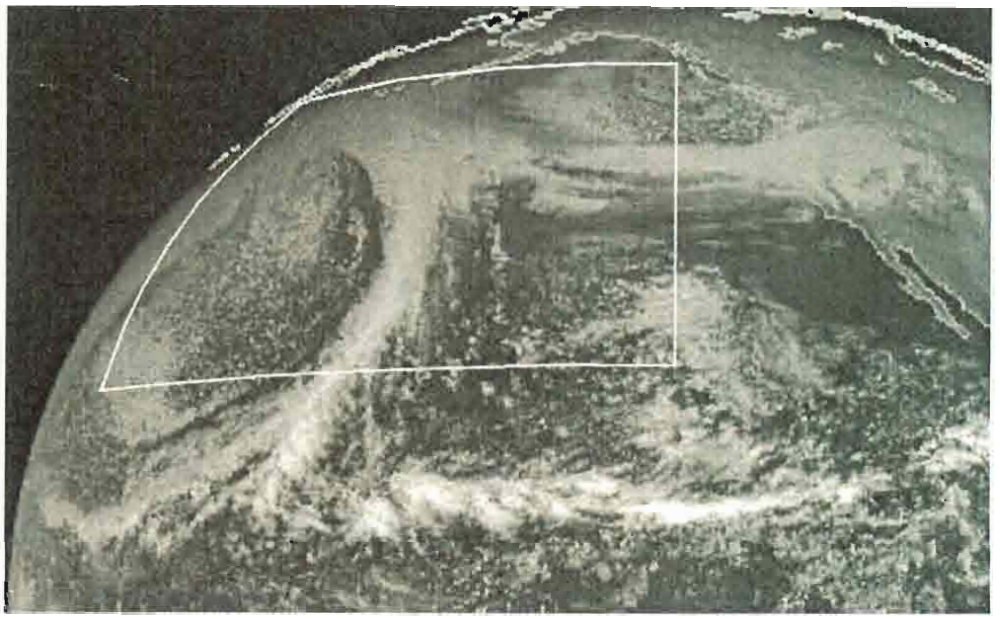

Figure 18. GOES-9 visible imagery from 1800 UTC 20 December 1996. Lines mark the study domain (20°N to 55°N and 165°E to 225°E).

time as figure 9). The cyclone is centered at 38°N and 186°E, as evidenced by the circulation center, high relative vorticity, and NCEP pressure field. A narrow band of high relative vorticity curves southeast from the center along the trailing cold front. NSCAT winds are southeast in front of this feature and west behind it. Rough contours of surface temperature made from NCDC ship and buoy data indicate a substantial temperature drop and tight horizontal gradients across the high vorticity line. Furthermore, GOES-9 visible imagery (figure 18) shows a classic comma head at the low pressure center and band of cloudiness along the trailing cold front. These two independent data sources confirm that the high vorticity band is indeed a signature of the cold front.

Warm and stationary fronts have strong NSCAT vorticity signatures similar to those of cold fronts. The NSCAT wind and relative vorticity fields from two passes of the satellite

Warm and stationary fronts have strong NSCAT vorticity signatures similar to those of cold fronts. The NSCAT wind and relative vorticity fields from two passes of the satellite

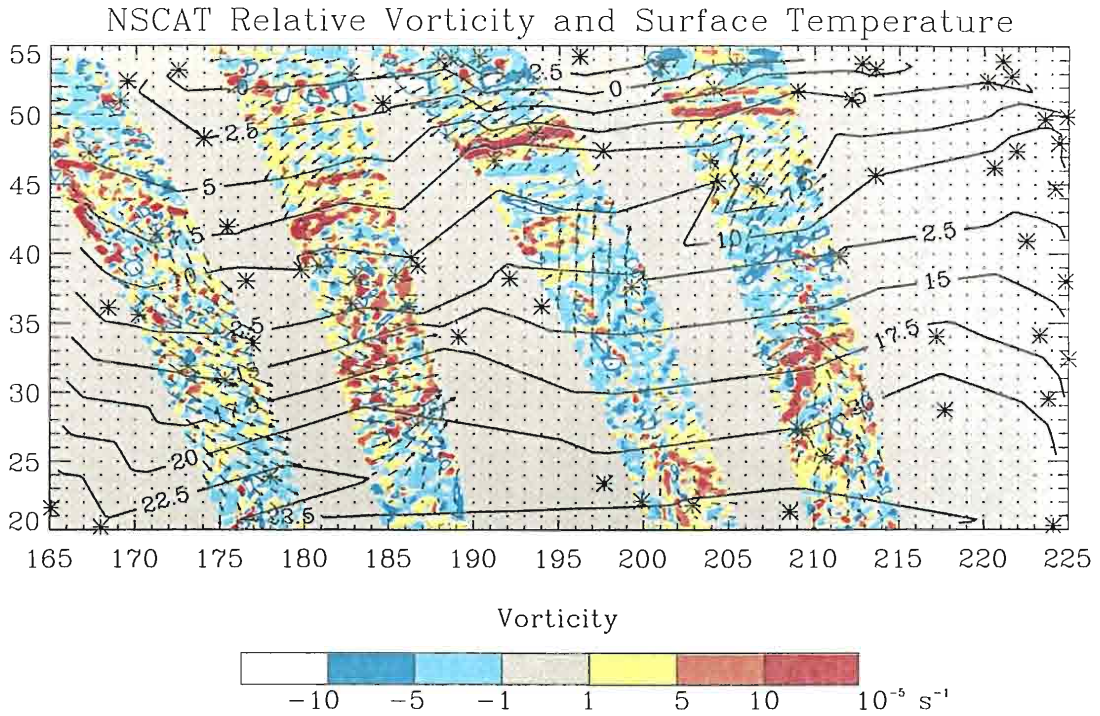

Figure 19. NSCAT winds and relative vorticity from 2 satellite passes around 1800 UTC 5 January 1997. Isotherms (°C) are from NCDC ship and buoy data (asterisks mark individual observations). Warm front extends from the cyclone center eastward across the northern portion of the domain.

around 1800 UTC 5 January 1997 (same time as figure 16) are plotted in figure 19. A developing cyclone (shown in the NCEP analyses) is centered near 42°N and 184°E, and a band of strong vorticity extends eastward from the center. There is a dramatic wind shift along this feature, with winds from the northeast on the north side and from the southwest on the south side. Surface temperature contours from NCDC data show strong temperature gradients from the high vorticity line northward. GOES-9 visible imagery from the same time (figure 20) shows dual cyclones in the domain. The western cyclone is seen in the NSCAT vorticity and winds, but there are no well-defined fronts in either NSCAT or GOES-9 data. The eastern cyclone has a broad band of cloudiness extending from the center eastward across the northern portion of the domain. This cloud band confirms the presence of the warm front that was first identified in the NSCAT vorticity. The NSCAT

center eastward across the northern portion of the domain. This cloud band confirms the presence of the warm front that was first identified in the NSCAT vorticity. The NSCAT vorticity field succeeds in locating the front within 25 to 50 km, the same order of

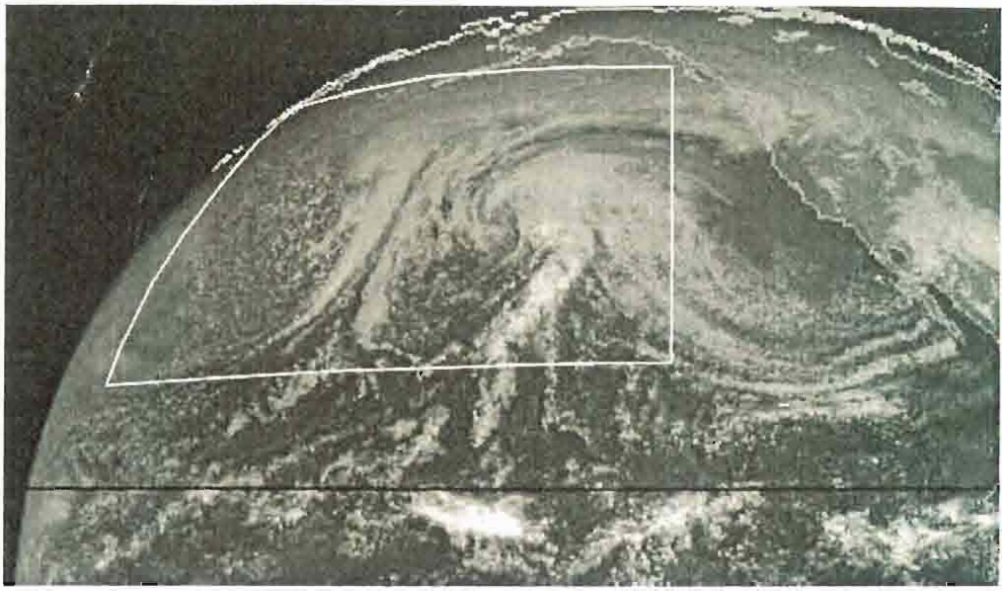

Figure 20. GOES-9 visible imagery from 1800 UTC 5 January 1997. Lines mark the study domain. Cloud band running east to west across the northern domain confirms the presence of a warm front.

magnitude as the resolution of the NSCAT winds and more exact than other satellite data sources.

CHAPTER 6

CONCLUSIONS

A variational method is devised to generate surface pressure fields from NSCAT winds. The method solves for a geostrophic stream function field by smoothly blending NSCAT relative vorticity with ambient geostrophic vorticity. The field is updated as new passes of the satellite over the study area provide additional information. Neumann boundary conditions, updated daily with NCEP gradients, allow the surface pressure field to evolve in time.

This method is used to study a case of cyclogenesis and a case of frontogenesis in the North Pacific. The NSCAT pressure fields correctly capture these features as they intensify and move through the study area. The NSCAT pressure fields are qualitatively compared to NCEP reanalyses mean sea level pressure, and both fields are quantitatively compared to NCDC ship and buoy observations. The domain-averaged differences between NSCAT pressures and surface observations range from 0.4 mb to 4.6 mb in magnitude with a standard deviation between 3.0 mb and 8.2 mb. NCEP pressures compare better, with mean differences below 1.2 mb in magnitude and standard deviations below 5.8 mb. The accuracy of the NSCAT pressure fields increases in recent satellite swaths and in recent swaths near the reference buoys.

Qualitatively, the NSCAT pressure fields resolve the structure of these systems more realistically and with greater detail than NCEP analyses. Also, the centers of cyclones are placed more accurately in the NSCAT pressure fields than in NCEP analyses, when compared to the centers of circulation from NSCAT winds. The average difference is 150

km for the NSCAT fields and 230 km for NCEP analyses.

Another result of this study is the signature of surface fronts in relative vorticity fields computed from NSCAT winds. Fronts are clearly identified by linear bands of high relative vorticity values. These bands are verified as fronts using surface temperature gradients and satellite imagery. NSCAT vorticity fields locate the fronts with an accuracy of 25 to 50 km and with greater resolution than other satellite data sources.

Although NSCAT winds are high quality data source, effective techniques for assimilation into NWP models have proven difficult to develop. Surface pressure fields from NSCAT winds, however, would provide a more favorable assimilation source [*Hoffman,* 1993; *Atlas*, 1998]. This study brings forth a simple method for determining surface pressures from NSCAT winds and demonstrates its effectiveness.

REFERENCES

Andrews, P. L. And R. S. Bell, Optimizing the United Kingdom Meteorological Office data assimilation for ERS-1 scatterometer winds, *Mon. Wea. Rev., 126,* 736-746, 1998.

Anthes, R. A., V. H. Kuo, and J. R. Gyakum, Numerical simulations of a case of explosive marine cyclogenesis, *Mon. Wea. Rev., 111,* 1174-1188, 1983.

Atlas, R., Atmospheric observations and experiments to assess thier usefulness in data assimilation, *Journ. Meteor. Soc. Japan, 75,* 111-130, 1997.

Bourassa, M. A., M. H. Freilich, D. M. Legler, W. T. Liu, and J. J. O'Brien, Wind observations from new satellite and research vessels agree, *EOS, 78,* 51, 1997

Bourassa, M. A., L. Zamudio, and J. J. O'Brien, Non-inertial flow in NSCAT observations of Tehuantepec winds, *J. Geophys. Res.,* submitted.

Boutin, J., and J. Etcheto, Consistency of geosat, SSM/I, and ERS-1 global surface wind speeds - comparison with in situ data, *J. Atmos. And Ocean. Tech., 13,* 183-197, 1996.

Brown, R. A., and L. Zeng, Estimating central pressures of oceanic midlatitude cyclones, *J. Appl. Meteor., 33,* 1088-1095, 1994.

Browning, K. A. And N. M. Roberts, Structure of a frontal cyclone, *Q. Journ. Roy. Meteor. Soc., 120,* 1535-1557, 1994.

Carlson, T. N., Air flow through midlatitude cyclones and the comma cloud pattern, *Mon. Wea. Rev., 108,* 1489-1509, 1980.

Carlson, T. N., *Mid-latitude weather systems*, 507 pp., HarperCollinsAcademic, London, Great Britian, 1991.

Clarke, R. H., and G. D. Hess, On the relation between surface wind and pressure gradient, especially in lower latitudes, *J. Phys. Oceanogr., 9,* 325-339, 1975.

Djuric', D., *Weather analysis,* 304 pp. Prentice-Hall, Inc.,Englewood Cliffs, New Jersey, 1994.

Djuric', D., *Weather analysis,* 304 pp. Prentice-Hall, Inc.,Englewood Cliffs, New Jersey, 1994.

Freilich, M. and R. S. Dunbar, A preliminary C-band scatterometer model function for the ERS-1 AMI instrument, *Proc. First ERS-1 Symp.*, Cannes, France, European Space Agency, 79-83, 1992.

Freilich, M. and R. S. Dunbar, The accuracy of NSCAT-1 vector winds: comparison with NCDC buoys, *J. Geophys. Res.*, submitted for NSCAT special issue, 1998.

Gonzales, A. E., and D. G. Long, An assessment of NSCAT ambiguity removal, *J. Geophys. Res.*, accepted, 1998.

Harlan, J. Jr., and J. J. O'Brien, Assimilation of scatterometer winds into surface pressure fields using a variational method, *J. Geophys. Res., 91,* 7816-7836, 1986.

Hoffman, R. N., A preliminary study of the impact of the ERS-1 C-band scatterometer wind data on the European Center for Medium-Range Weather Forecasts global data assimilation system, *J. Geophys. Res., 114,* 515-543, 1993.

Jones, W. L., L. C. Schroeder, D. H. Boggs, E. M. Bracalante, R. A. Brown, G. J. Dome, W. L. Pierson, and F. J. Wentz, The Seasat-A satellite scatterometer: The geophysical evaluation of remotely sensed wind vectors over the ocean, *J. Geophys. Res., 87,* 3297-3317, 1982.

Liu, W. T., W. Q. Tang, and P. S. Polito, NASA scatterometer provides global ocean-surface wind fields with more structures than numerical weather prediction, *Geophys. Res. Letters, 25,* 761-764, 1998.

Long, D. G. And J. M. Mendel, Model-based estimation of wind fields over the ocean from scatterometer measurements part I: the wind field model. *IEEE Trans. Geosci. Remote Sens., GE-27,* 268-276, 1991.

Offiler, D., The calibration of ERS-1 satellite scatterometer winds, *J. Atmos. Ocean. Technol., 11,* 1002-1017, 1994.

Renka, R., Interolation of data on the surface of a sphere, *Oak Ridge Nat. Lab. Rep. OLNR/CSD-108,* 1982.

Rufenach, C., Comparison of four ERS-1 scatterometer wind retrieval algorithms with buoy measurements, *J. Atmos. Ocean. Tech., 15,* 304-313, 1998.

Sasaki, Y., Some basic formalisms in numerical variational analysis, *Mon. Wea. Rev., 108,* 875-883, 1970.

Stoffelen, A. and D. Anderson, Ambiguity removal and assimilation of scatterometer data, *Q. J. Roy. Meteor. Soc., 123,* 491-518, 1997.

Q. J. Roy. Meteor. Soc., 123, 491-518, 1997.

Thepaut, J. N. R. N. Hoffman, and P. Courtier, Interactions of dynamics and observations in a four-dimensional variational assimilation, *Mon. Wea. Rev., 121,* 3393-3414, 1993.

Tommassini, M., D. LeMeur, and R. W. Saunders, Near-surface satellite wind observations of hurricanes and their impact on ECMWF model analyses and forecasts, *Mon. Wea. Rev., 126,* 1274-1286, 1998.

Verschell, M. A., M. A. Bourassa, D. E. Weissman, and J. J. O'Brien, Model validation of the NASA scatterometer winds, *J. Geophys. Res.,* submitted.

BIOGRAPHICAL SKETCH

The author was raised in Panama City, Florida, where he attended Bay High School. After graduating in 1982 as a member of the academic top ten, he studied pre-engineering at Gulf Coast Community College in Panama City. From there he enrolled in the University of Florida and studied civil engineering for three years. No degree was earned, as studies were eventually abandoned for a career in the restaurant business.

After working in different restaurants in Gainesville, Florida over several years, the author moved to Tallahassee, Florida to pursue a degree from Florida State University's Department of Meteorology. A Bachelor of Science degree was awarded in April 1997. While attending the university, he was employed part-time as a Data Quality Evaluator at FSU's Center for Ocean-Atmospheric Prediction Studies (COAPS).

After graduation, the author continued his education in pursuit of a Master's of Science degree in meteorology. Studies were under the direction of Dr. James J. O'Brien at COAPS. He also worked part-time as a research assistant and was coauthor of a paper published in *The Bulletin of the American Meteorological Society*, "Are Gulf Hurricanes Getting Stronger?" This thesis is partial fulfilment of master's degree requirements and will be submitted for publication in the *Journal of Geophysical Research.*